International Journal of Pharmaceutics 635 (2023) 122716

Contents lists available at ScienceDirect

International Journal of Pharmaceutics

journal homepage: www.elsevier.com/locate/ijpharm

Oral empagliflozin-loaded tri-layer core-sheath fibers fabricated using tri-axial electrospinning: Enhanced *in vitro* and *in vivo* antidiabetic performance

Ece Guler [a,b,c,1], Ayse Nur Hazar-Yavuz [a,1], Esra Tatar [d], Mohammad Morid Haidari [a], Gul Sinemcan Ozcan [e], Gokhan Duruksu [e], Manuel Pedro F Graça [f], Deepak M Kalaskar [c], Oguzhan Gunduz [b,g], Muhammet Emin Cam [a,b,c,h,i,*]

[a] Department of Pharmacology, Faculty of Pharmacy, Marmara University, Istanbul 34854, Turkey
[b] Center for Nanotechnology and Biomaterials Application and Research, Marmara University, Istanbul 34722, Turkey
[c] UCL Division of Surgery and Interventional Science, Royal Free Hospital Campus, University College London, Rowland Hill Street, NW3 2PF, UK
[d] Department of Pharmaceutical Chemistry, Faculty of Pharmacy, Marmara University, Istanbul 34854, Turkey
[e] Stem Cell and Gene Therapies Research and Applied Center, Medical Faculty, Kocaeli University, Kocaeli 41380, Turkey
[f] I3N and Physics Department, University of Aveiro, 3810-193 Aveiro, Portugal
[g] Department of Metallurgy and Material Engineering, Faculty of Technology, Marmara University, Istanbul 34722, Turkey
[h] Biomedical Engineering Department, University of Aveiro, 3810-193 Aveiro, Portugal
[i] Genetic and Metabolic Diseases Research and Investigation Center, Marmara University, 34854 Istanbul, Turkey

ARTICLE INFO

Keywords:
Type 2 diabetes mellitus
Empagliflozin
Core-sheath fiber
Insulin resistance
Tri-axial electrospinning

ABSTRACT

Empagliflozin (EM) was successfully loaded in polycaprolactone/poly (L-lactic acid)/polymethyl methacrylate (PCL/PLA/PMMA) fibers. In the rat β-cell line (BRIN-BD11), the insulin expression ratio of pancreatic β-cells was stimulated at high and low glucose by culturing with tri-layer EM-loaded fiber (EMF) for 48 h. The expression ratios of glucokinase and GLUT-2 proteins increased after EMF treatment. According to the *in vitro* drug release test, 97% of all drug contained in fibers was released in a controlled manner for 24 h. The pharmacokinetic test revealed that the bioavailability was improved ~4.8-fold with EMF treatment compared to EM-powder and blood glucose level was effectively controlled for 24 h with EMF. Oral administration of EMF exhibited a better sustainable anti-diabetic activity even in the half-dosage than EM-powder in streptozotocin/nicotinamide-induced T2DM rats. The levels of GLP-1, PPAR-γ, and insulin were increased while the levels of SGLT-2 and TNF-α were decreased with EMF treatment. Also, EMF recovered the histopathological changes in the liver, pancreas, and kidney in T2DM rats and protected pancreatic β-cells. Consequently, EMF is suggested as an unprecedented and promotive treatment approach for T2DM with a higher bioavailability and better antidiabetic effect compared to conventional dosage forms.

1. Introduction

Diabetes Mellitus (DM) is one of the most important diseases that can cause serious side effects and even death. DM is characterized by chronic hyperglycemia as a result of impairment in protein, carbohydrate, and fat metabolism caused by insulin resistance or deficiency in insulin secretion and exhibits elevated glycosylated hemoglobin A1C (Cam et al., 2020; Glovaci et al., 2019). It may occur with symptoms such as blurred vision, polyuria, polydipsia, thirst, and weight loss. In addition to chronic hyperglycemia, it causes acute and chronic complications such as neuropathy, coma, nephropathy, retinopathy, cardiovascular and cerebrovascular diseases, and ketoacidosis, especially because of its damage to the nerves, veins, and organs over time. There are two major types of diabetes: Type 1 and type 2 diabetes. Type 1 diabetes (T1DM) is caused by a complete loss in insulin secretion capacity as a result of autoimmune destruction of β cells in the pancreas, while type 2 diabetes (T2DM) is characterized by a decreased insulin sensitivity in the skeletal muscle, adipose tissue, and liver (Alberti and Zimmet, 1998; DeFronzo,

* Corresponding author at: Department of Pharmacology, Faculty of Pharmacy, Marmara University, Istanbul 34854, Turkey.
E-mail address: muhammet.cam@marmara.edu.tr (M. Emin Cam).
[1] Contributed equally to this work.

https://doi.org/10.1016/j.ijpharm.2023.122716
Received 11 September 2022; Received in revised form 6 February 2023; Accepted 8 February 2023
Available online 13 February 2023

1999; Fonseca et al., 2000; Imagawa et al., 2000; Nathan, 1993).

According to the data on DM prevalence, it is a global health crisis that has increased from approximately 30 million to 135 million patients in 10 years and is expected to reach 300 million by 2025 (Hjelm et al., 2003). The World Health Organization (WHO) predicts that DM will be the seventh cause of death in 2030 (Mathers and Loncar, 2006). In addition, the estimated numbers of adults that have T1DM, T2DM, and other DM types in 2016 were 1.3 million, 21.0 million, and 0.8 million according to the National Health Interview Survey (NHIS), respectively (Bullard et al., 2018; Zghebi et al., 2017).

The pathophysiology of DM, which is one of the most serious and chronic diseases affecting a large population with acute and chronic complications worldwide, continues to be investigated nowadays. There are five major oral antidiabetic drug groups used to treat the currently known pathophysiology of T2DM: a) Drugs that delay the absorption of glucose - α-glycosidase inhibitors, b) insulin-releasing drugs - sulfonylureas and benzoic acid derivatives (glinides), c) drugs to reduce insulin resistance - biguanides and thiazolidinedione derivatives, d) incretin mimetic drugs - dipeptidyl peptidase-4 inhibitors (DPP4-I) and glucagon-like peptide-1 receptor agonists (GLP-1A), and e) sodium-glucose co-transporter-2 (SGLT-2) inhibitors (Çubuk and İnce, 2015; Modi, 2007) Empagliflozin (EM), which is a strong and selective inhibitor of SGLT-2, has approved for the treatment of T2DM in 2014 by Food and Drug Administration (FDA). The mechanism of action of EM in T2DM treatment is to increase urinary glucose excretion by decreasing the reabsorption of filtered glucose inhibiting the SGLT-2 receptors in kidneys regardless of cell function and insulin resistance. Thus, it leads to a decrease in the level of plasma glucose due to this mechanism (Barnett et al., 2014; Tikkanen et al., 2015). On the other hand, EM protects diabetic pancreatic cells by inhibiting the activation of the nucleotide-binding oligomerization domain-like receptor protein 3/caspase-1/ Gasdermin D pathway in pancreatic β cells (Liu et al., 2021).

Nanotechnology is one of the most important technological developments in the areas of chemistry, biosensor, biotechnology, bioelectronics, genetic engineering, tissue engineering, and medicine to produce controllable nanoscale materials usually 100 nm or smaller with new functions and features such as having high surface–volume ratio, which provides higher activities for them in surface-related phenomena compared to bulky systems of the same mass (Alenezi et al., 2021; Farokhzad and Langer, 2009; Nasrollahzadeh et al., 2019; Papadopoulos and Taghiyari, 2019). The development of nanotechnology has brought innovation to science in drug delivery systems. High drug loading capacity and efficiency, homogeneity in the size of the drugs, and long-term and therapeutic drug delivery could be given as examples of these developments in nanotechnology (Park, 2007).

Electrospinning (ES), which has a special principle based on using the interaction between the working fluid and electrical energy is preferred as a common technology for the production of micro or nano-scaled fibers (Zhao et al., 2021). A metal needle system is preferred as a spinneret that belongs to the ES process for collecting a polymeric solution towards an electrically grounded collector roll as a fiber by being exposed to a high electric voltage. However, using one metal needle is one of the biggest problems, especially in the case of the needle clogging alongside being cumbersome and slow. Therefore, multi-needle spinnerets have been invented to overcome the clogging problem, provide to produce multiple-chamber nanostructures, and generate sustained release medicated nanofibers by using core and sheath solutions (Martin et al., 2022; Panić et al., 2022; Partheniadis et al., 2022; Wang et al., 2023; Wang et al., 2020).

The concentric spinneret, working fluids, and suitable working conditions are very important for the fabrication of core-sheath fibers, which is the most popular one among electrospun multiple-chamber nanostructures (Jiang et al., 2022). Firstly, a spinneret for producing a two-layer nanofiber has been developed by using two different solutions. The whole circle of the spinneret was fully charged by these two fluids. In this system, two working fluids can not have any connection point in the two-parallel metal capillary format however, they can contact each other through an enlarged surface area of the capillary system. After that, this two-layer nanofiber production method was further improved by pumping three working fluids for creating the three-layer nanofibers (Liu et al., 2022b). The tri-axial electrospinning (tES) is a technique used in the production of small-diameter fibers ranging from micron size to 100 nm (Yu et al., 2023). Ceramic, metal, polymer, and composite could be used as materials in this production technique (Frenot and Chronakis, 2003; Ramakrishna, 2005; Teo and Ramakrishna, 2006). The three working fluids in tES exhibit great potential to produce core–sheath fibers. In this system, the unspinnable solvent can be utilized as an outer working fluid to make easier the production of functional fibers compared to traditional single-fluid electrospinning (Zhou et al., 2022). Furthermore, this unspinnable solvent has a positive influence on the convenience between the two other working fluids by decreasing the difficulty of the production of core–-sheath fibers (Liu et al., 2022c). In addition, nanofibers produced from polymers create an environment suitable for the targeting of drugs and showing the rapid onset of drug effects. Moreover, polymers provide drugs to be released as showing controlled, rapid, and sustained release properties from nanofibers (Ogueri and Laurencin, 2020; Verma et al., 2010). Therefore, exhibiting sustained drug release provides reduced administration time, keeps a constant blood drug concentration, and shows safer therapeutic effects for patients (Liu et al., 2022a).

The oral administration route is the most suitable and preferred way of administration due to the several advantages compared to other routes of administration. These advantages are painless and easy application, economically cheap, no special training for drug utilization, high patient compliance, low immune system response, and maintaining drug absorption along the gastrointestinal tract. To take the advantage of both oral administration and fiber dosage form, EM was loaded in tri-layer nanofibers to be applied by oral route for the treatment of T2DM (Shahriar et al., 2019; Verma et al., 2010).

The denaturation problems of the one-layer fibers are reduced by increasing the number of fiber layers and thus, inner layers and their components are protected from electric charges during tES. In addition, the increased porosity, expanded surface area, and improved cell adhesion are provided by using bioactive surface groups. Therefore, polycaprolactone (PCL), poly (L-lactic acid) (PLA), and polymethyl methacrylate (PMMA), which are FDA-approved and hydrophobic polymers, were used in the inner, middle, and outer layers of core-sheath fibers, respectively. PMMA is a low-cost thermopolymer and improves the mechanical strength of nanotechnological products whereas, PLA and PCL are biodegradable, biocompatible, bioabsorbable, hydrophobic, and synthetic polymers (Aydin et al., 2022; Pandey et al., 2019; Rashahmadi et al., 2017). EM-powder degrades quickly in the bloodstream and acidic gastric juice. Therefore, the metabolic instability and poor water solubility of EM restrict its practical clinical application. For this reason, EM was loaded in PCL in the inner layer. Thus, the controlled release of the drug and its protection from the acidic environment of gastric juice was provided by choosing the hydrophobic polymers in the production of core-sheath fiber and loading the drug in the inner layer (Alenezi et al., 2019; Ghoroghchian et al., 2006; Hrkach et al., 1996; Mishra et al., 2020; Shimko and Nauman, 2007; Sperling et al., 2016; Tang et al., 2005; Xie et al., 2022).

It was aimed to increase the effect of EM on the targeted tissue by loading in tri-layer PCL/PLA/PMMA fibers in the present study. Hereby, side effects will be reduced and the solubility, pharmacokinetic, and pharmacodynamic profiles of the drug will be improved. In addition, the characterization tests of the solutions used in the production of fibers; *in vitro* drug release kinetics, degradation and swelling, SEM, DSC, FTIR, XRD, tensile, and *in vitro* cell culture tests of the fibers were performed, and *in vivo* animal studies, biochemical, and histological analysis were done to investigate the antidiabetic activity of the fibers. A schematic illustration of the study was given in Fig. S1, Supporting Information.

2. Materials and methods

2.1. Materials

Poly (L-lactic acid) (PLA) 2003D was obtained from Nature Works LLC, Minnetonka, MN. Polycaprolactone (PCL, Mw ~ 80,000 g mol^{-1}), polymethyl methacrylate (PMMA, Mw ~ 120,000 g mol^{-1}), streptozotocin (STZ, Mw ~ 265.2 g mol^{-1}), empagliflozin (EM, Mw = 450.9 g mol^{-1}), chloroform, barbital, acetonitrile, and phosphate buffer saline (PBS, pH = 7.4) were purchased from Sigma-Aldrich (Poole, UK). Orthophosphoric acid and triethanolamine were kindly provided by Dermo Clean Laboratories (Istanbul, Turkey). All these materials were of the analytical grade. ELISA kits were purchased from Bioassay Technology Laboratory, Korain Biotech Co., Ltd (Shanghai, China).

2.2. Preparation and characterization of solutions

Three different solutions were prepared using PCL, PLA, and PMMA polymers to produce tri-layer PCL/PLA/PMMA fibers. PCL was dissolved in a mixed solvent (chloroform:methanol, 3:1, v/v) at the concentration of 10% (w/v) by stirring using a magnetic stirrer for an hour at room temperature. PMMA was mixed for 2 h at 60 °C in chloroform at 20% (w/v). PLA was dissolved in chloroform at the concentration of 8% (w/v) by stirring at room temperature for an hour. EM at a concentration of 8.4 mg/ml was added to the PCL core solution for the production of EM-loaded PCL/PLA/PMMA nanofibers (EMF). It was stirred at room temperature for an hour. Physical parameters such as density, electrical conductivity, surface tension, and viscosity were measured for the solutions by using the electrical conductivity probe (Cond 3110 SET 1, WTW, Germany), standard density bottle (10 ml, Boru Cam Inc., Turkey), viscometer (DV-E, Brookfield AMETEK, USA), and force tensiometer (Sigma 703D, Attension, Germany), respectively. All the measurements were repeated three times at ambient temperature. These equipments were calibrated prior to measurements.

2.3. Preparation and characterization of fibrous mats

The pure nanofibers and tri-layer EMF were produced at room temperature by tES (NS24, Inovenso Co., Turkey) using three concentrically nested needles. The outer (OD) and inner diameters (ID) of the inner, middle, and outer needles were (OD:1.47 mm, ID:1.07 mm), (OD: 2.13 mm, ID: 1.88 mm), and (OD: 3 mm, ID: 2.87 mm), respectively. PCL, PLA, and PMMA were used for the inner, middle, and outer layers, respectively. Other components of the equipment included three syringe pumps (New Era Pump Systems, Inc., USA), a high-voltage power supply, and a rotating collector wrapped with wax paper, which is employed as a collector. Distance ranges, flow rate, and different voltages were applied for the production of tri-layer PCL/PLA/PMMA fibers and the most suitable parameters were selected for each layer. The morphologies and diameters of fibers were analyzed using SEM. Thus, the core-sheath fibers which have the best properties were produced.

2.4. Scanning electron microscopy (SEM)

Fiber diameters and morphological characteristics of electrospun pure fibers and tri-layer EMF were evaluated using scanning electron microscopy (SEM) (EVO LS 10, ZEISS, USA). The surfaces of the fiber samples were coated with palladium and gold using the sputter coater (SC7620, Quorum) to render them electrically conductive for 120 s before investigating with SEM. Afterward, 100 fibers for each sample were selected to determine the average fiber diameter by using image software ImageJ (Brocken Symmetry Software).

2.5. Focused ion beam-scanning electron microscopy (FIB-SEM)

The cross-sectional morphologies of the samples were analyzed by a focused ion beam-scanning electron microscope (FIB–SEM) using a Hitachi ETHOS NX5000. A rough beam (12 nA) was utilized to cut a section with a depth of 10 μm and length of 11 μm. After that fine etching was performed on the cross-section for analysis using a mid-beam (1.5 nA) to cut a length of 10 μm and a depth of 5 μm. The applied accelerating voltage to take the cross-sectional SEM images was 20–30 kV and the working distance was 4 mm. The AFM images were obtained on a Bruker Dimension Icon utilizing the ScanAsyst mode. An AFM probe (Bruker, Model: TAP525A) providing a resonant frequency of 525 kHz and a spring constant of 200 N/m was used.

2.6. X-Ray powder diffraction (XRD)

Cu Kα radiation and D / Max-BR diffractometer (RigaKu, Tokyo, Japan) were used to analyze the crystal forms and structures of the raw materials (PCL, PLA, PMMA, and EM), pure fiber, and tri-layer EMF. After that, analyses were performed at 40 mV and 30 mA over 2θ range of 5–80° at a rate of 2°/min, and the data obtained using the OriginPro 7.0 software (OriginLab Corporation, MA, USA) was converted in diffractograms.

2.7. Fourier-transform infrared spectroscopy (FTIR)

FTIR (Jasco, FT / IR 4700) was used to evaluate the chemical structures and contents of pure fibers and tri-layer EMF. It was evaluated whether PCL, PLA, PMMA, and EM were loaded successfully in the fibers. Measurements were obtained between 500 and 4000 cm^{-1} wavenumbers with a resolution of 4 cm^{-1} at room temperature. OPUS Viewer version 6.5 software was used during the analysis.

2.8. Tensile tests of fibers

After the tensile strength of core-sheath fibers was determined at room temperature by using an Instron 4411 tensile testing machine and then, it was analyzed with Bluehill 2 software (Elancourt, France). It was tested by taking three samples from each fiber sample (10 × 50 mm). The thickness of the samples was measured using a digital micrometer (Mitutoyo MTI Corp., USA). Both ends of each sample were compressed by the top and bottom grip and the tensile test was performed on a 5 mm min^{-1} test speed and 10 mm distance between grips.

2.9. Differential scanning calorimeter (DSC)

The thermal properties of the core-sheath fibers were determined under a dynamic argon atmosphere (20 ml min^{-1}) at a heating rate of 10 °C min^{-1} between 0 and 200 °C by using Perkin Elmer Jade DSC and Pyris software (PerkinElmer Inc., Mass., USA). Temperature calibration of DSC was performed according to the indium melting point and melting enthalpy.

2.10. Drug encapsulation efficiency

Encapsulation efficiency (EE) was described as the actual amount of drug loaded in fibers / theoretical amounts of the drug in fiber. A standard assay procedure was used to define the EM content inside the fibers. Briefly, the core-sheath fibers dissolved completely in their mixture of solvents, and detection was actualized by UV at 267 nm (Padmaja et al., 2018). EMF was weighed (5 mg) and dissolved in 10 ml of their solvent mixtures in a volumetric flask. The flask was gently mixed for an hour to completely dissolve EM from the core-sheath fibers into the solvent mixtures. 1 ml of solution was taken and detected by using a UV–visible spectrophotometer at 267 nm (Shimadzu UV-3600, Japan). All measurements were repeated in triplicate.

2.11. In vitro EM release kinetic assay

Firstly, EM was prepared in 5 different concentrations (2, 4, 6, 8, and 10 μg/ml) to construct a linear calibration curve. The analysis was performed to investigate the release kinetics of EM from core-sheath fibers. EMF was cut into an average weight of 5 mg each and then firstly, it was immersed to pH 1.2 (for 2 h), then transfer to pH 6.8 (for 2 h), and subsequently to pH 7.4. It was held on a rotary shaker that was set to 250 rpm and 37 °C to evaluate the drug release kinetics for a period of 48 h. PBS was removed from each sample at the scheduled times (0, 0.25, 0.5, 1, 2, 3, 4, 6, 8, 12, 24, and 48 h) and 1 ml of fresh PBS was added again to continue the release test. UV spectroscopy (Shimadzu UV-3600, Japan) was used for analyzing the EM releasing profile at 267 nm (Javanbakht et al., 2019; Padmaja et al., 2018).

2.12. In vitro EM release kinetics

Five different mathematical models were used to simulate the EM release kinetics from the core-sheath nanofibers. These kinetic models are Korsmeyer-Peppas, zero-order, first-order, Higuchi, and Hixson Crowell models (Aguzzi et al., 2010). The equations belonging to the drug release kinetic mathematical models are below (Table 1):

In these equations, Q is the fractional amount of drug release at time t; K, K_0, K_1, K_h, and K_{hc} are the kinetic constants for Korsmeyer-Peppas, zero-order, first-order, Higuchi, and Hixson-Crowell models, respectively. n is the diffusion exponent which is indicative of the drug release mechanism.

2.13. In vitro degradation test

The degradation test of nanofibers was performed using conventional methods. Briefly, the dried nanofibers were cut into small square pieces. Each cut specimen was exactly measured for the initial weight (~5 mg). Then, firstly, they were immersed in 1 ml of HCl for 2 h for simulating stomach acid, and then, it was continued with PBS (pH 7.4) in a 37 °C shaking incubator for up to 41 days. The PBS solution was changed after each measurement with fresh one. Specimens were removed at 1, 4, 8, and 12 h, and on days 5, 9, 13, 17, 21, 24, 29, 33, 37, and 41. The water on the surface was gently removed with filter paper after the removal of the specimens. Then specimens for each time point were weighed and subsequently dried in a vacuum until a constant weight was obtained. The degradation of mass loss (%) was calculated as follows:

$$Degradation\ \ test(\%) = [(Wb - Wt)/Wb] \times 100$$

where W_b is the original weight, and Wt is the weight of the degraded sample at incubation time (t).

2.14. In vitro swelling test

The swelling behavior of nanofibers was evaluated by measuring the initial weight of the dry samples and then, nanofibers were immersed in PBS (pH 7.4, 37 °C) for different periods of time intervals (0.5, 1, 2, 3, 8, and 24 h). Three replicates were performed for each sample. Before measuring the weight of the swollen samples, the water on the surface was gently removed with filter paper after the removal of the samples. The swelling ratio was calculated using the following equation:

$$Swelling\ \ ratio : (Wt - Wb)/Wbx100$$

where W_b is the original weight, and Wt is the weight of the swollen sample at incubation time (t).

Table 1
The drug release kinetic mathematical models and their equations.

Kinetics Model	Equations
Korsmeyer-Peppas	$Q = Kt^n$
Zero-order	$Q = K_0 t$
First-order	$\ln (1 - Q) = -K_1 t$
Higuchi	$Q = K_h t^{1/2}$
Hixson Crowell	$Q^{1/3} = K_{hc} t$

2.15. Cell proliferation assay (WST)

To conduct the assay, nanofibers were first cut into circular sheets (5 mm in diameter) and pre-incubated in 200 μl per sheet of DMEM (Thermo, Gibco, Paisley, UK) supplemented with 10 % fetal bovine serum (Thermo, Gibco) and %1 Pen-Strep (Thermo, Gibco) for 24 h at 37 °C. This conditioned medium was later used for cytotoxicity assay. Human fibroblast cells were seeded in 96-well plates at a density of 1.0×10^4 cells per well (n = 6) and incubated in DMEM at 37 °C in a humidified atmosphere of 5 % CO_2 for 24 h. The medium was removed completely and replaced with 200 μl of conditioned medium. After the incubation of cells for 48 h at 37 °C in the humidified atmosphere of 5 % CO_2, cell viabilities were evaluated with quantification of their metabolic activity using the WST-1 cell proliferation assay (Roche, Mannheim, Germany) according to the instructions of the manufacturer. Briefly, the medium was replaced with 10 % WST-1 solution in DMEM, and the cells were incubated for 2 h at 37 °C. The formation of the soluble formazan dye can be quantified with the measurement of absorbance at 450 nm. The cell viability was expressed as a percentage of control cultures (performed in DMEM without the conditioning with nanofiber).

2.16. In vitro cell culture

The effect of EM on insulin expression was analyzed on rat β-cell line, BRIN-BD11. BRIN-BD11 cells were cultured in DMEM/F12 (Gibco, Thermo, Paisley, UK) supplemented with 10% FBS (Gibco) and 1% penicillin–streptomycin (Gibco) under the standard culture condition at 37 °C in a humidified atmosphere with 5% CO_2. After cells reached 70–80% confluency, cells were passaged by 0.25% trypsin-EDTA (Gibco), and reseeded on the new culture dish at a 1:3 ratio.

The basal medium (DMEM/F12) contains 5.5 mM glucose (low glucose medium). To induce insulin secretion by glucose, the basal medium was supplemented with D-glucose (high glucose medium) to obtain the final glucose concentration of 25 mM. To observe the difference in insulin expression at different glucose concentrations, the cells were cultured for 48 h. The effect of pure fibers and EMF were compared on the cells cultured in both low and high-glucose media.

The effect of EM on β-cells was evaluated by the expression analyses of insulin (Ins), glucokinase, and glucose transporter (GLUT) proteins. Total RNA was extracted by Aurum Total RNA Mini Kit (Bio-Rad, Hercules, CA) using the protocol supplied by the manufacturer. cDNA was generated by iScript cDNA Synthesis Kit (Biorad) using the protocol supplied by the manufacturer. The gene expression was evaluated by using iTaq Universal SYBR Green Supermix (Biorad) in LightCycler 480-II system (Roche). PCR amplification followed a two-step cycling program: 30 s pre-denaturation at 95 °C, 45 cycles at 95 °C for 15 s, and 60 °C for 60 s. Cp values were determined by LightCycler 480 Software (release 1.5). ActB gene amplification was used as a housekeeping gene in the calculations.

2.17. In vivo test

All *in vivo* experiments were approved with the permission of Marmara University Animal Experiments Local Ethics Committee (permission number: 77.2019.mar). Adult female and male Sprague Dawley rats (225–250 g) at the age of 3–4 months were obtained from Marmara University, The Experimental Animal Implementation and Research Centre. The rats were placed in a controlled temperature (20 ± 2 °C),

humidity (40–60%), and 12 h dark/light cycle-regulated rooms with free access to standard rodent food and tap water. All necessary precautions were taken before the experiment and the factors that could negatively affect the parameters were diminished during the study.

2.17.1. Induction of T2DM

32 Sprague Dawley rats were fasted for 12 h and then administrated with nicotinamide (NA) (100 mg/kg, solved in saline) for once to minimize STZ-induced pancreatic β-cell damage. 15 min later, rats were injected with STZ (55 mg/kg, solved in 0.1 M citrate buffer, pH = 4.5) to induce diabetes 72 h after injection, blood samples were taken from the tail vein of rats and high blood glucose levels (BGL) was measured using a glucometer (Contour Plus, Bayer Diagnostics). The rats that have BGL above 200 mg/dL were considered T2DM. Later on, 8 rats were taken for the pharmacokinetic study, and the remaining 24 rats were taken for the antidiabetic activity test. All treatments have begun and lasted for 21 days in the antidiabetic activity test for analyzing the antidiabetic effect of EMF with the comparison of EM powder (Badole et al., 2015; Cam et al., 2019).

2.17.2. Pharmacokinetic study

2.17.2.1. Pharmacokinetic evaluation of EMF. The amount of EM released from EMF was determined for 72 h by high performance liquid chromatography (HPLC). After EMF (5 mg/kg) and EM-powder (10 mg/kg) intragastric (i.g.) administrations to the rats, 0.5 ml of blood samples were collected from the *retro*-orbital plexus at the scheduled times (0 and 30 min; 1, 2, 4, 6, 8, 12, 24, 48, and 72 h) to detect the amount of EM and measure BGL. The glucose measurement was performed using Contour™ TS, Bayer Diagnostics blood glucose meter (Shewamene et al., 2015).

The area under the curve (AUC) for serum EM level was calculated using GraphPad Prism 8.0 statistical program. Cmax and tmax were determined from AUC. The relative bioavailability (BA_R) was calculated. BA_R of nanofibers after oral administration was calculated using the following equation:

$$BA_R = \frac{AUC_{(nanofiber)} \text{ x } Dose_{(powder)}}{AUC_{(powder)} \text{ x } Dose_{(nanofiber)}} x100\%$$

where AUC is the total area under the plasma insulin concentration vs. time curve.

2.17.2.2. Experimental scheme for pharmacokinetic evaluation. There are randomly divided into 2 groups for the pharmacokinetic evaluation and 4 animals in each test group as follows: Powder Group (EM): Diabetic rats were given a single dose of 10 mg/kg/day (i.g.) of EM (Michel et al., 2015). Fiber Group (EMF): Diabetic rats were given a single dose of 5 mg/kg/day (i.g.) of EMF.

2.17.2.3. Chromatographic conditions. The liquid chromatographic system used consisted of an Agilent Technologies 1200 series instrument equipped with a quaternary solvent delivery system, Agilent series G-13158 photodiode array detector, and G1367B Agilent 1200 Series high-performance autosampler. Chromatographic data were collected and processed using HP-Vectra VL-DOO DT software.

The separation was performed at ambient temperature on a reversed-phase KROMASIL 100-5C18 column (4.6 mm × 150 mm, 5 μm particle size). A Waters Symmetry C18 analytical guard column packed with the same sorbent was used. The mobile phase consisted of the acetonitrile: triethanolamine phosphate buffer solution (30: 70, pH 3.0) delivered at a flow rate of 1.0 ml/min. The injection volume was 50 μl. The analytes were monitored using a PDA detector at 230.4 nm.

Preparation of triethanolamine-phosphate buffer: 1 ml triethanolamine was dissolved in 1000 ml bidistilled water. The final pH of the solution was adjusted to 3.0 with orthophosphoric acid. Stock solutions of EM and barbital (internal standard): 1 mg of each was weighed and dissolved in 100 ml methanol and preserved at + 4 °C. The working solutions were freshly prepared by the appropriate dilution of the stock solutions with the mobile phase containing 200 ng/ml of barbital in each solution as an internal standard with EM in the range of 50–500 ng/ml.

2.17.2.4. Plasma sample preparation. 200 μl of plasma samples and 200 μl of barbital solution were taken into the tube. The mixture was vortexed for 2 min, and 1 ml of tetrahydrofuran was added into the tube. Subsequently, the samples were vortexed for 3 min and centrifuged for 10 min at 10000 rpm. The supernatant was filtered through a 0.2 μm syringe filter, and 600 μl of the mobile phase was added and transferred into an HPLC vial.

Calibration curves were constructed from plasma samples spiked with 200 ng/ml of barbital solution and EM solutions of 50–500 ng/ml.

2.17.2.5. Method validation. The validation of the method was carried out by performing specificity, linearity, limit of quantification (LOQ), precision, accuracy, recovery, and matrix effect experiments. The specificity was analyzed by comparing the chromatography of blank rat samples with that of the EM-spiked rat plasma samples.

The linearity was studied using the concentrations of EM in rat plasma at 50, 100, 200, 500, 1000, 2000, 5000, and 10000 ng /ml. LOD samples were prepared at a concentration of 50 ng/ml. Quality control (QC) samples were performed in three respects low, medium, and high concentrations (50, 500, and 5000 ng/ml) to evaluate the precision and accuracy of the method.

The recovery of the QC and IS samples were obtained by calculating the peak area ratio between the peak areas of extracted analytes and those of the reference solutions added to the extracted blank plasma samples. The matrix effect was evaluated by comparing the response of EM (50, 500, and 5000 ng/ml) and barbital (200 ng/ml) in the rat matrix with respect to that in the solvent.

2.17.3. Antidiabetic activity test

2.17.3.1. Experimental scheme for antidiabetic activity test. There are randomly divided into 4 groups in the antidiabetic activity test and 6 animals in each test group as follows: Control Group (C): Pure fibers were given to healthy rats (in the same size with EMF per day, i.g.). Diabetes Group (DM): Pure fibers were given to diabetic rats (in the same size with EMF per day, i.g.). Fiber Treatment Group (DM + EMF): Diabetic rats were given EMF (5 mg/kg/day, i.g.). Powder Treatment Group (DM + EM): Diabetic rats were given EM-powder (10 mg/kg/day, i.g) (Michel et al., 2015).

EM was dissolved in saline and given to rats in the DM + EM group (10 mg/kg/day in 5 ml/kg). Pure fibers were given to the C and DM groups in the same size as drug-loaded fibers. EM-powder and EMF were given to rats using stainless steel gavage needles. EM concentration was 2 times higher in the DM + EM group (10 mg/kg) compared to the DM + EMF group (5 mg/kg). The antidiabetic efficiency of EMF, which released EM in a sustained manner for up to 24 h (97% of all EM) according to *in vitro* drug release test, was compared with EM-powder, which was the currently used form of EM in the treatment of T2DM. All these treatments were given for 21 days. A schematic illustration of the *in vivo* study was given in Fig. S2, Supporting Information.

2.17.3.2. Determination of body weight and BGL. Body weight and BGL of all groups were measured weekly and blood samples were collected from the tail vein for monitoring BGL using a glucometer.

2.17.3.3. Oral glucose tolerance test (OGTT). OGTT is a commonly used clinical test to diagnose glucose intolerance and T2DM. After 12 h of fasting, treatments were applied and 30 min later, a single dose of 2 g/kg glucose was given by oral gavage. Glucose concentrations were

monitored in the blood taken from the tail vein at 0, 30, 60, and 120 min following the glucose injection (Cam et al., 2017).

2.17.3.4. Insulin tolerance test (ITT). After 12 h of fasting, treatments were administered and insulin was injected into rats (1 U/kg, i.p.). BGLs from blood samples taken from the tail vein were measured using a glucometer at 0, 30, 60, 90, 120, 150, and 180 min following the insulin injection (Boland et al., 2019).

2.18. Biochemical analysis

Pancreas, liver, kidney, and intestinal tissue samples were collected after decapitation. After the rat tissues were homogenized, biochemical analyzes were performed using ELISA kits from Bioassay Technology Laboratory, Korain Biotech Co., Ltd (Shanghai, China). All procedures were made in compliance with the instructions of the manufacturer.

2.19. Histological analysis

To examine the light microscopic analysis, the liver, pancreas, and kidney tissues obtained were quickly washed with saline and fixed for 72 h in 10% neutral buffered formalin after the experimental animals were sacrificed. Tissues were then dehydrated by passing through increasing alcohol series (70%, 90%, 96%, and 100%), cleared in xylene for 2x10 min, and embedded in paraffin. Hematoxylin and Eosin (H&E) staining was applied to perform the morphological evaluation on sections taken from paraffin blocks about 4 μm thick, then, sections were examined by light microscopy (LEICA DM 1000) and photographed.

2.20. Immunohistochemistry analysis

Immunohistochemistry for insulin in pancreas tissues was performed as follows: The sections were deparaffinized followed by rehydration in a graded series of alcohols, and then immersed in 3% H_2O_2 to suppress endogenous peroxidase activity, and microwaved in 10 mM sodium citrate (pH 6.0) for 20 min for antigen retrieval. Then, avidin and biotin were applied to eliminate endogenous biotin-related background staining. The sections were then incubated with primary antibody (anti-insulin (ab181547)) or PBS (negative control) at 4 °C overnight and incubated, respectively, with a biotinylated secondary antibody and HRP-conjugated streptavidin (ABCAM, ab236466) for 15 min at room temperature. The slides were washed and the chromogen was developed for 5 min with liquid 3,30-diaminobenzidine (DAB) before observation. Contrasting staining with hematoxylin was performed. The expression of both primary antibodies was photographed under light microscopy.

2.21. Statistical analysis

SEM results are presented as mean ± standard deviation. The interactions between different groups in cell culture and animal tests were studied using analysis of variance (ANOVA) with a 95% confidence interval and Tukey's post hoc test. The results were expressed as mean ± standard error of the mean, and values of p greater than 0.05 were not considered significantly different, whereas values of $p < 0.05$ were considered significant. Data analysis was performed using GraphPad Prism 8.0 software (GraphPad, San Diego, CA, USA).

3. Results

3.1. Physical properties of solutions

Different solutions were prepared for the production of EMF and pure core-sheath fiber. The distance, voltage, and flow rate are among the key factors that change the diameter, homogeneity, and structure of the core-sheath fibers produced using tES. The solution properties are affected by viscosity, density, surface tension, and electrical conductivity (Alfares et al., 2021; Ibrahim et al., 2019). PCL (10% w/v), PLA (8% w/v), and PMMA (20% w/v) were prepared for the production of tri-layer fibers and EM was loaded in the PCL layer. After the addition of EM in the PCL solution, density increased from 1.30 g/ml to 1.32 g/ml and the surface tension decreased from 24.2 mN/m to 22.5 mN/m. The viscosity increased from 4030 mPas to 5980 mPas, while the electrical conductivity decreased from 3.3 μS/cm to 1.5 μS/cm. The density, surface tension, electrical conductivity, and viscosity of PLA are 1.44 g/ml, 26.50 mN/m, 2 μS/cm, and 290 mPas, respectively. The density of PMMA is 1.435 g/ml, and the surface tension and the viscosity are 35.2 mN/m and 3944 mPas, respectively. Electrical conductivity could not be measured for PMMA. The core-sheath fiber diameter increased after loading of EM in core-sheath fibers. The viscosity, surface tension, and density increased while the electrical conductivity decreased in the PCL solution by adding EM (Fig. S3, Supporting Information).

3.2. Morphological characterization of fibers

The tri-layer nanofibers were consisted of PCL (10%, w/v), PLA (8%, w/v), and PMMA (20% w/v) from the inner to the outer layer, respectively, and EM was loaded in the PCL layer. The fibers were produced by tES using three concentrically nested needles. After the addition of EM in fibers, the diameter of fibers increased from 773.1 ± 195.5 to 961.0 ± 443.2 nm.

The distance, voltage, and flow rate parameters were changed to produce the core-sheath fibers. The flow rate for the PCL layer was applied between 0.1 and 0.8 ml/h during the production of pure fibers. It was tried between 0.8 and 1.5 ml/h for PLA and PMMA layers. On the other hand, the distance was tested between 12 and 18 cm, and the voltage was applied between 12 and 25 kV for all three layers. The most suitable pure fiber production was obtained at the flow rate of 0.1 ml/h for PCL, 1.2 ml/h for PLA, and 1.2 ml/h for PMMA. The applied voltage and working distance for pure fibers were 20 kV and 15 cm, respectively. After loading EM in the PCL layer, the distance remained constant, while the voltage increased to 25 kV. The flow rate was determined as 0.1 ml/h, 1.3 ml/h, and 3.5 ml/h for PCL, PLA, and PMMA, respectively. Thus, fiber production without beads in suitable diameters and morphological structures was successfully carried out in these parameters (Fig. 1a-b).

The internal structure of tri-layer EMF was examined using FIB-SEM. Fig. 1c demonstrated the SEM images of a cross-section obtained by cutting via FIB. Following the FIB section, it can clearly be seen that the fibers were successfully produced and demonstrated three distinct layers by the thickness of 85, 95, and 770 nm from outer to inner, respectively. Each layer is labeled accordingly in Fig. 1c and d.

3.3. X-Ray powder diffraction (XRD)

XRD results show that three peaks at $2\theta = 21.4°$, 22.0°, and 23.5° demonstrate the semi-crystalline nature of PCL (Fig. S4a, Supporting Information) (Abdelrazek et al., 2016; Liu et al., 2018). Pure PMMA exhibits four different amorphous peaks at $2\theta = 15.0°$, 22.49°, 30.0°, and 41.41° (Fig. S4b, Supporting Information) (Abdelrazek et al., 2016; Devikala et al., 2016). Major peaks at $2\theta = 14.52°$, 18.6v4°, 20.18°, and 25.0° demonstrate the crystal nature of EM (Fig. S4c, Supporting Information) (Niguram et al., 2020). Pure PLA shows a semi-crystalline nature and gives characteristic peaks at $2\theta = 12.5°$, 14.7°, 16.6°, 19.1°, and 22.3° (Fig. S4d, Supporting Information) (Chew et al., 2013; Kaczmarek et al., 2013). According to XRD results, it was shown that PCL, PMMA, and PLA polymers were practically loaded in all fiber samples (Fig. S4e, Supporting Information). Different peaks were observed in EM-loaded core-sheath fiber compared to pure core-sheath fiber due to the crystal structure of EM. Thus, it was proved that EM was successfully loaded in fibers (Fig. S4f, Supporting Information).

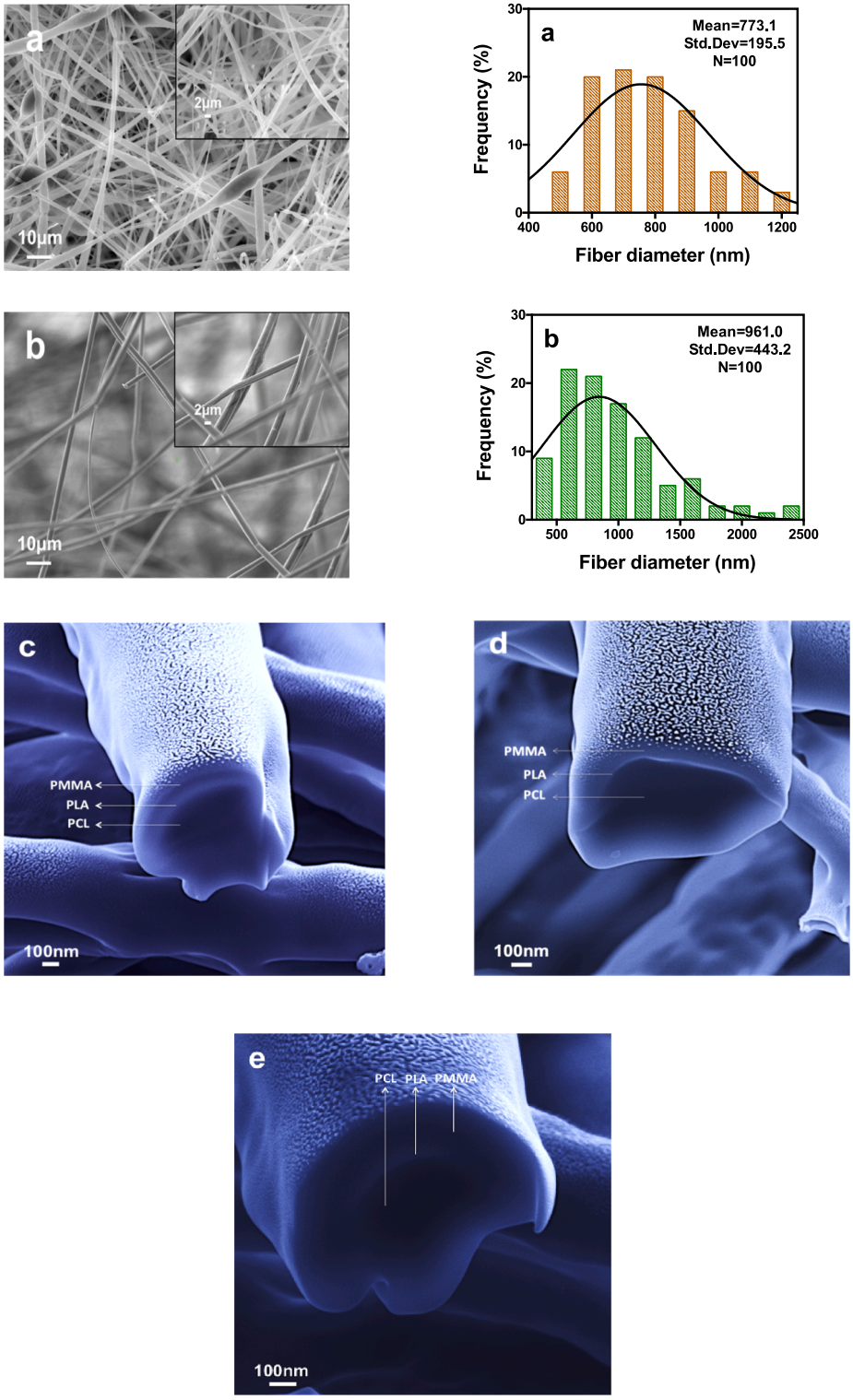

Fig. 1. SEM images and fiber diameter distributions of pure and EM-loaded fibers produced by using tES: (a) Pure fibers, (b) EM-loaded fibers. In all diameter distributions, and (c, d, and e) FIB-SEM image of EM-loaded fibers, n = 100.

3.4. Fourier-transform infrared spectroscopy (FTIR)

The molecular structures of pure PCL, PMMA, PLA, EM, pure fiber, and EMF were shown in Fig. S5, Supporting Information. The band of C = O stretching vibration of PLA was detected at 1745 cm^{-1}. Bending vibrations of CH_2 for PLA are observed in the range of 1300–1500 cm^{-1} and the bands of C-O-C stretching vibrations and backbone vibration with CH_3 rocking mode were observed at 1181 cm^{-1} and 866 cm^{-1}, respectively (Pamuła et al., 2001). The C = O stretching band for carbonyl group of PCL were located around 1727 cm^{-1} while the symmetrical and asymmetrical stretching bands of CH_2 were observed at 2943 cm^{-1} and 2864 cm^{-1}, respectively. The stretching bands of C–C and C-O groups were obtained at 1294 cm^{-1} and 1167 cm^{-1}, respectively (Khatiwala et al., 2008). In the spectra of pure PMMA, the

characteristic C–H asymmetric and symmetrical stretching bands were detected at 2978 cm^{-1} and 2877 cm^{-1}, respectively, and the C–H vibration bands at 1387 cm^{-1} and 1456 cm^{-1} were also observed. C-O-C band due to ether moiety was also seen at 1025 cm^{-1}. Furthermore, the band of C = O groups for pure PMMA was observed at 1730 cm^{-1} (Khan et al., 2008). In the spectra of EM, OH-free stretching bands, OH-bonded stretching bands, C–H stretching bands, aromatic C = C bands, and C-O-C deformation bands were seen at 3977–3815 cm^{-1}, 3479 cm^{-1}, 2874 cm^{-1}, 1616–1504 cm^{-1}, 997–775 cm^{-1}, respectively (Bhole and Tamboli, 2018). In the IR spectrum of pure and EM-loaded core-sheath fiber, the bands at 2944. cm^{-1}, 2865 cm^{-1}, and 1722 cm^{-1} were attributed to pure PCL while the band at 1365 cm^{-1} was attributed to PLA. The bands appertaining to PMMA were seen at 1434 cm^{-1} and 1394 cm^{-1}. The bands at 1294 cm^{-1} and 1159 cm^{-1} belonging to PCL were also observed. Additionally, the characteristic bands for EM were observed at 2980 cm^{-1}, 1720.19, and 1066 in only EMF's IR spectrum. Thus, this revealed that EM was loaded successfully.

3.5. Tensile test of fibers

Tensile strength, strain at break, and stress–strain curve of samples were given in Fig. 2a-c. It was determined that pure fiber has greater tensile strength than EMF. Tensile strength decreased from 195.5 ± 26 kPa to 84.2 ± 21 kPa after loading the drug in pure fibers. Furthermore, it was observed similar outputs in the results of strain at break. In addition, after loading EM in pure fibers, fiber diameters increased and it was observed that the tensile strength and strain at break decreased.

3.6. Differential scanning calorimetry (DSC)

In Fig. 2, the DSC curves of fibers were examined between 0 and 200 °C. Fig. 2d shows the DSC curve of pure fiber. Apparently, the glass transition temperature (Tg) of PLA is seen around 60 °C, and the melting temperature (Tm) of PCL is also observed at the same temperature as the Tg value of PLA. For this reason, it is hidden under the PCL endotherm (Kelnar et al., 2016). On the other hand, the Tm value of PLA was obtained between 150 and 180 °C whereas, the Tg of PCL is noticed at approximately −61.5 °C (Aydin et al., 2022; Wachirahuttapong et al., 2016). Therefore, it could not be evaluated in the current working range. PMMA shows no melting steps and crystallization because of its fully amorphous structure (Mangin et al., 2020).

The Tm value of EM is exhibited at around 152 °C (Niguram et al., 2020). Therefore, the pure fiber exhibited Tg and Tm endothermic peaks at 64.6 °C and 155.3 °C in Fig. 2d. The working temperature ranges between Tg and Tm slightly decreased to 61.5 °C and 151.7 °C after loading EM. In the case of comparing EMF and pure fibers, the reason for this drop in Tg and Tm temperatures may be due to the physical or chemical interactions between EM and polymers or the crystal structure of EM.

3.7. In vitro drug release

In vitro drug release kinetic assays for tri-layer EMF were done and examined at five different release kinetic models. In the beginning, five different concentrations of EM between 2 and 10 μg/mL were prepared at and measured by UV spectra (Fig. 3A-a). The linear standard calibration curve was constructed from EM absorption values ($R^2 = 0.9693$) obtained for the quantitative determination of drug release (Fig. 3A-b). The released EM was detected by UV at 267 nm. Moreover, the EE of EM loaded in tri-layer fibers was calculated by 89.3 ± 4.5% (Fig. 3A-c). Afterward, *in vitro* drug release test was performed to investigate the releasing profile of encapsulated EM in core-sheath fiber in PBS by mimicking the pH of the simulated gastric fluid (pH 1.2, at 37 °C), the first zone of intestinal fluid (pH 6.8, at 37 °C), and the second intestinal zone fluid and plasma (pH 7.4, at 37 °C) for 48 h.

It is seen in Fig. 3A-d, all of the EMF demonstrated a burst drug release by releasing 42.8% in the first 30 min. Furthermore, 97% of all drug contained in fibers was released in a controlled manner in 24 h compared with the first 30 min. In pharmacokinetic evaluation, EM-powder lost its blood glucose lowering effect in 24 h while EMF showed longer blood glucose lowering effect by its sustained release profiles for 48 h. Consequently, EMF exhibited a longer release time, better protection against drug release at low pH, and a controlled release in the alkali conditions due to its strong degradation mechanism caused by the hydrophobic character and tri-layer structure of PCL/PLA/PMMA nanofiber (Javanbakht et al., 2019).

3.8. In vitro drug release kinetics

The different release kinetic models are the Korsmeyer-Peppas, zero-order, first-order, Higuchi, and Hixson-Crowell were used to evaluate the release kinetic of EM from core-sheath nanofibers (Table 2). The results showed that EM with higher R^2 values (0.8637) was released from core-sheath nanofibers according to the Hixson-Crowell release model (Fig. 3B). Hixson–Crowell model is described as a system in which the surface changes by time and the cube root of the released amount of the encapsulated drug are linearly related to time (Aydin et al., 2022; Jahromi et al., 2020).

Furthermore, the values of n that corresponds to different transport mechanisms were used to characterize the Korsmeyer–Peppas release model. The range of n values was exhibited in Table 3. The range of n value was found between $0.45 < n < 0.89$ in this study. Thus, it was shown that EM was released from nanofibers through the Non-Fickian transport mechanism.

3.9. In vitro degradation test

In this study, PLA, PCL, and PMMA polymers were used in the production of nanofibers due to their biodegradable properties. Therefore, their features make polymer metabolizations easier in medical applications used in the human body (Dong et al., 2009). Fragmentation and hydroxylation of high molecular weight chains of PCL perform with/without enzyme in the degradation mechanism of PCL (Meng et al., 2010). In addition, the degradation process of PLA and PMMA is due to the hydrolysis of the functional group of ester and thermal degradation, respectively (Ferriol et al., 2003; Zong et al., 2003). On the other hand, nanofibers that have thinner diameters degrade faster due to larger surface area (Shao et al., 2011). Therefore, pure nanofibers exhibited faster degradation than EMF in the study. The degradation test for pure fibers and EMF lasted for 6 weeks. 37.8% and 34.5% of pure nanofibers and EMF degraded at the end of the 41 days, respectively. In addition, the movement of EM, which is a water-soluble drug, from nanofibers was restricted by hydrophobic polymers used in the production of nanofibers. In that case, sustained release of EM could have resulted from the degradation mechanism (Liu et al., 2016). The mass loss evaluation of the nanofibers during their degradation process was shown in Fig. 4a.

3.10. In vitro swelling test

The swelling behavior is an important parameter for the characterization of nanofibers. The swelling ratio of nanofibers is highly dependent on surface area contact with water molecules, porosity, and the average diameters of nanofibers (Xu et al., 2016). Moreover, the presence of hydroxyl groups in the chemical structure of components of nanofiber makes water molecules easily penetrate into nanofiber (Entekhabi et al., 2016). In addition, the rate of swelling behavior also affects the drug release behavior of nanofibers (Lee and Fu, 2003). In this study, pure tri-layer nanofibers have quite low water absorption values due to their hydrophobic structure. The swelling ratios of the pure nanofibers and EMF were found as 496.6% and 839.2%, respectively. The reasons for the higher swelling ratio belonging to EMF

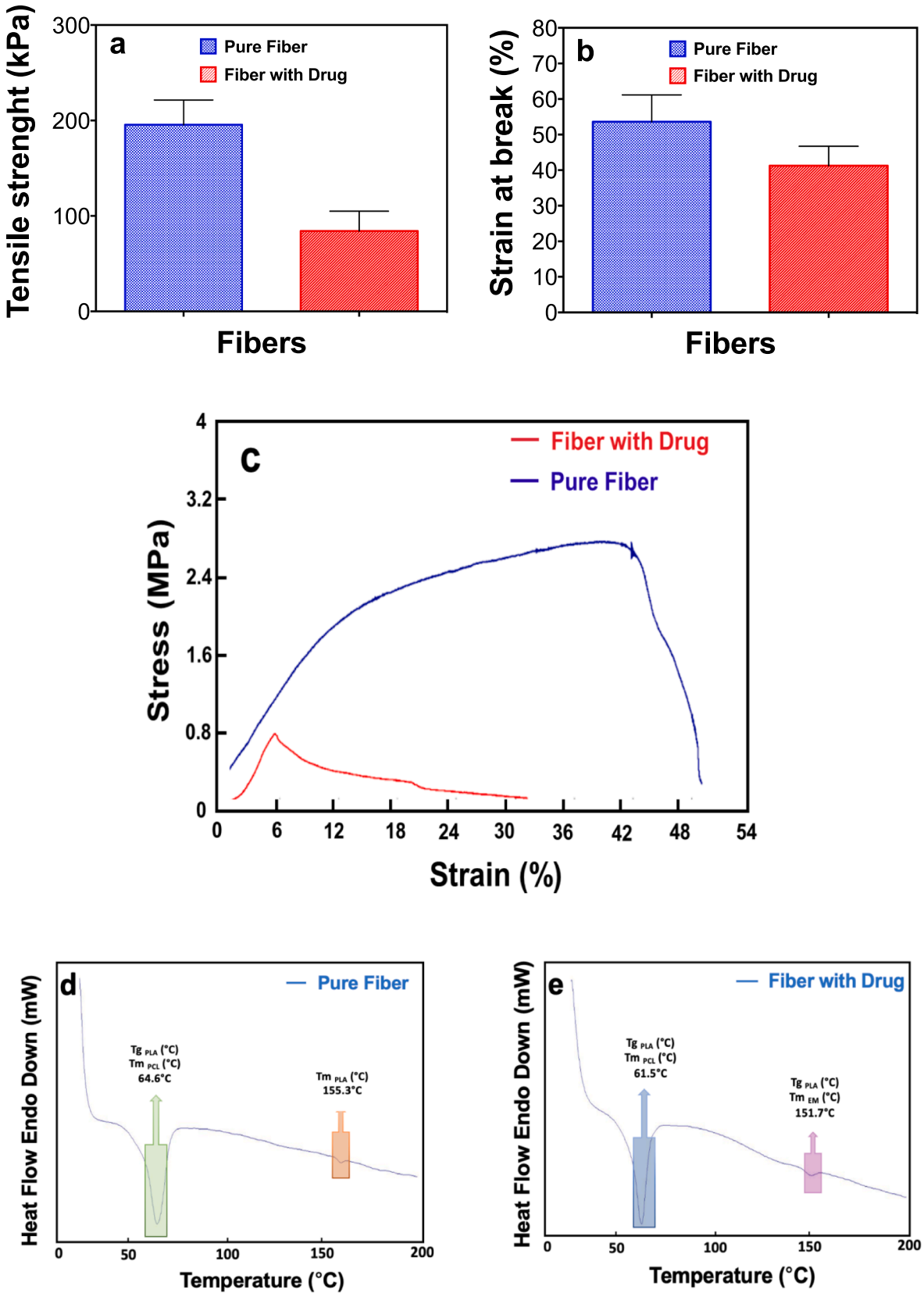

Fig. 2. Tensile properties of fibers: (a) Tensile strength, (b) strain at break, (c) stress–strain curve. DSC results of fibers: (d) Pure PCL/PLA/PMMA fiber and (e) EM-loaded PCL/PLA/PMMA fiber.

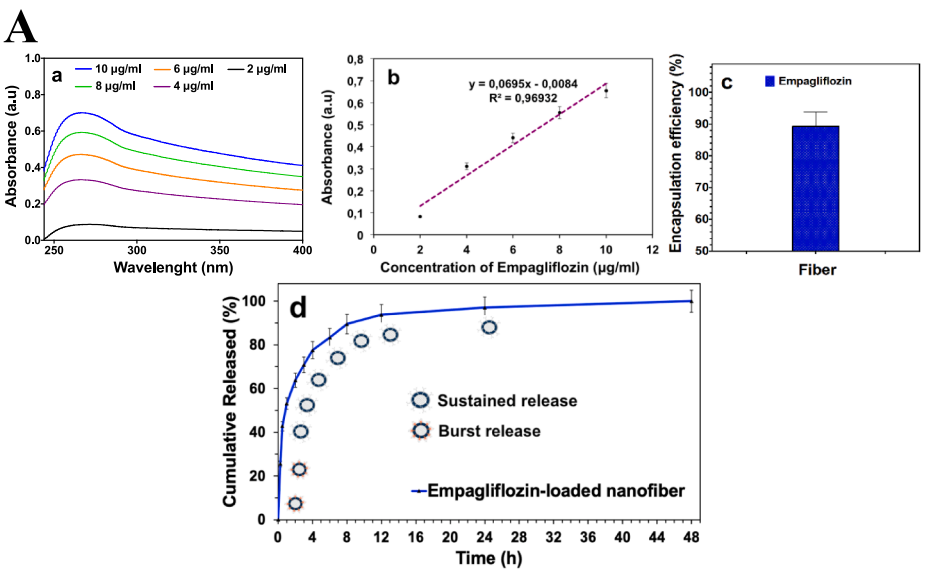

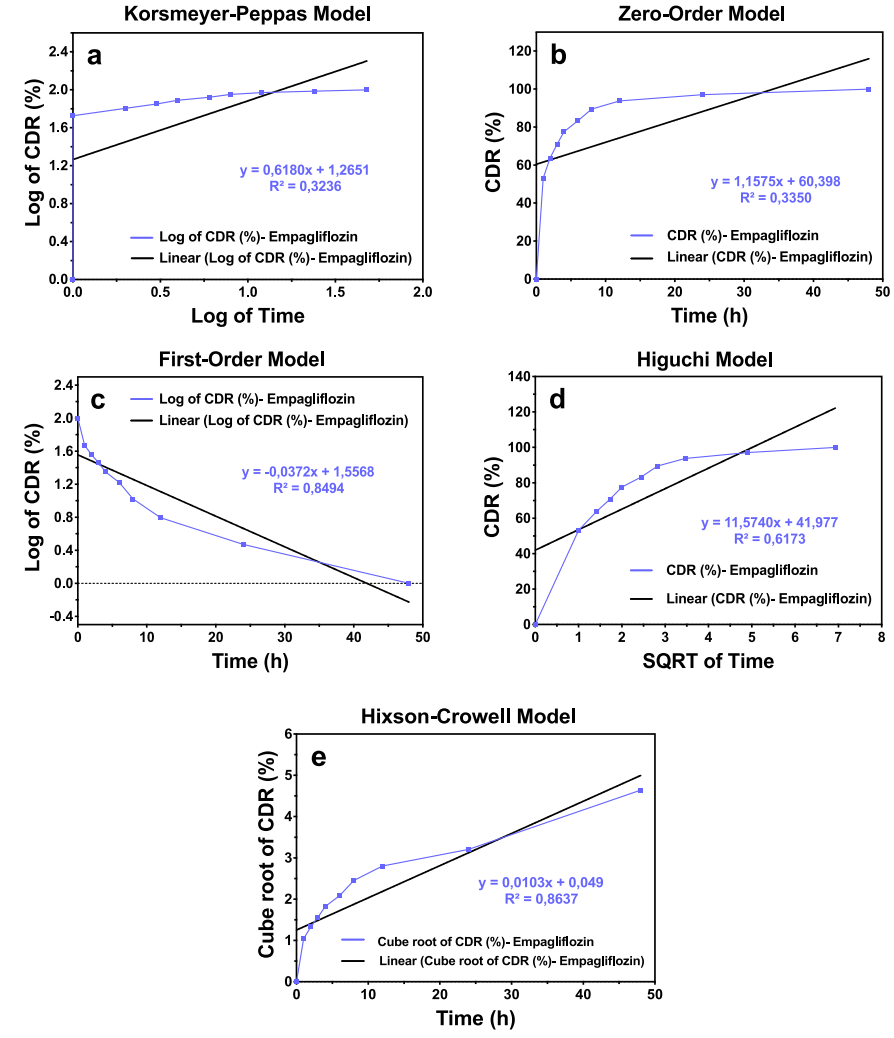

Fig. 3. A. *In vitro* drug release profile of EM-loaded PCL/PLA/PMMA fiber: (a) Absorption spectra of EM at different concentrations, (b) EM calibration curve, (c) Encapsulation efficiency of EMF, and (d) EM release profiles within 48 h. All the measurements were repeated three times and the errors were less than 5%. **B.** The release kinetic models of EM from PCL/PLA/PMMA core-sheath nanofibers: (a) Korsmeyer-Peppas, (b) zero-order, (c) first-order, (d) Higuchi, and (e) Hixson-Crowell models.

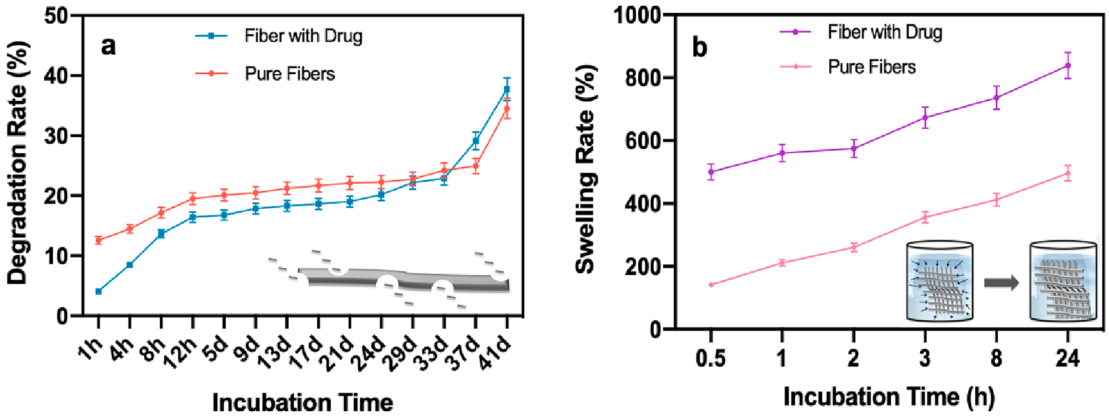

Fig. 4. (a) *In vitro* degradation test of pure and EM-loaded PCL/PLA/PMMA nanofibers and (b) *in vitro* swelling behavior of samples in different time intervals. The tests were performed by taking three samples from each nanofiber. Data represent the mean ± standard error of the mean (n = 3).

Table 2
Results of drug release kinetic models for all nanofibers. EM: Empagliflozin released from EM-loaded PCL/PLA/PMMA nanofibers.

	Korsmeyer-Peppas		Zero-Order		First-Order		Higuchi		Hixson-Crowell	
Sample	R^2	n	R^2	K_0	R^2	K_1	R^2	K_h	R^2	K_{hc}
EMF	0.3236	0.6180	0.3350	1.1575	0.8494	−0.0372	0.6173	11.5740	0.8637	0.0103

Table 3
Transport mechanism types according to the ranges of n value.

The ranges of n values	Transport Mechanisms
$0.45 \leq n$	Fickian diffusion mechanism
$0.45 < n < 0.89$	Non-Fickian transport
$n = 0.89$	Case II (relaxational) transport
$n > 0.89$	Super case II transport

compared to pure nanofibers are hydroxyl groups of EM and increased fiber diameters. The swelling ratios increased by 6 and 9 times compared to their initial weights of pure nanofibers and EMF, respectively, were shown in Fig. 4b.

3.11. Cell proliferation assay (WST)

Pure nanofibers and EMF were analyzed to determine whether they have any cytotoxic effect on human fibroblast cells. After 48 h of culture, the number of living cells was measured by spectrophotometer and the cell viability of fibroblast cells in the medium that has pure fiber (101.8 ± 5.0 %) has shown no significant difference compared to the control culture. On the other hand, the cell viability of culture that has EMF reduced to approximately 93.4% compared with control cells but there is no significant difference between the groups (Fig. 5a).

3.12. Cell culture

The effects of pure nanofiber and EMF were analyzed on rat pancreatic β-cell lines (BRIN-BD11). Pure nanofiber does not affect the expression of insulin or the glucose sensor proteins (glucokinase and GLUT-2). At high glucose concentrations, BRIN-BD11 cells expressed glucose transporter-2 (GLUT-2) and glucokinase proteins 2.0-fold and 2.4-fold higher than cells cultured at low glucose concentrations, respectively. The induction of expression of these two proteins provides to increase in pancreatic β-cells, Ins1, and Ins2, by 2.1- and 1.6-fold in high glucose medium. The effect of EM on rat pancreatic β-cells was found that it is significant. In the low glucose media that has EMF, GLUT-2 and glucokinase expressions were increased by 2.3- and 3.0-fold compared with control cultures. In the same culture, the expressions of Ins1 and Ins2 were induced by 2.1- and 1.7-fold, respectively, without the effect of the high glucose concentration. At the 25 mM glucose concentration, cells cultured with EMF demonstrated a 2.7- and 4.4-fold increase in the expression of GLUT-2 and glucokinase, respectively. In parallel to the expression of these two proteins, the expression of Ins1 and Ins2 was further induced by 4.6- and 2.7-fold under the effects of EMF and high glucose media compared with the cells cultured in the low glucose media without EM or fiber (Fig. 5b-c).

3.13. Pharmacokinetic evaluation

The calibration curve of EM evaluated the equation y 105941.x (R^2 0.9957) with high linearity throughout the concentration range of 50–500 ng/ml. The retention time for barbital and EM were recorded at the range of 2.94 and 9.95 min, respectively.

The relative standard deviation (RSD) of the intra-day and inter-day precision was less than 2%. The recovery of EM at 50, 500, and 5000 ng/ml concentrations ranged from 95%, 98%, and 102%, respectively and the RSD of each concentration was less than 2%. The matrix effect of EM at 50, 500, and 5000 ng/ml concentrations ranged and the internal standard was 93%, 95%, and 98% respectively. In conclusion, the method was accurate and applicable for determining the concentration of EM in rat plasma.

The plasma EM concentration–time profiles, reduction of initial glucose levels vs. time, and the pharmacokinetics parameters were shown in Fig. 6a, 6b, and Table 4, respectively.

In the EM group, the BGL was reduced for 4 h till 40.5 ± 4.0 % of its initial BGL and then started to increase. The decrease returned to 61.3 ± 4.9 % after 24 h and reached its beginning level in 48 h. As expected, EM-powder lost its blood glucose-lowering effect in 24 h. On the other hand, a longer blood glucose lowering period was achieved with EMF and BGL decreased to 35.9 ± 3.9 % of its initial level in 6 h and then started increasing to 40.2 ± 4.1 % in 24 h. After 48 h, BGL increased to 58.3 ± 5.4 % of its initial BGL and this phenomenon revealed that a sustained release was achieved with EMF for 48 h. The blood glucose lowering effect disappeared after 48 h and EM could not be detected in blood samples of the EMF group. The same situation occurred in 24 h for the rats treated by EM-powder. The release time was longer with the EMF group due to the strong hydrophobic character and tri-layer

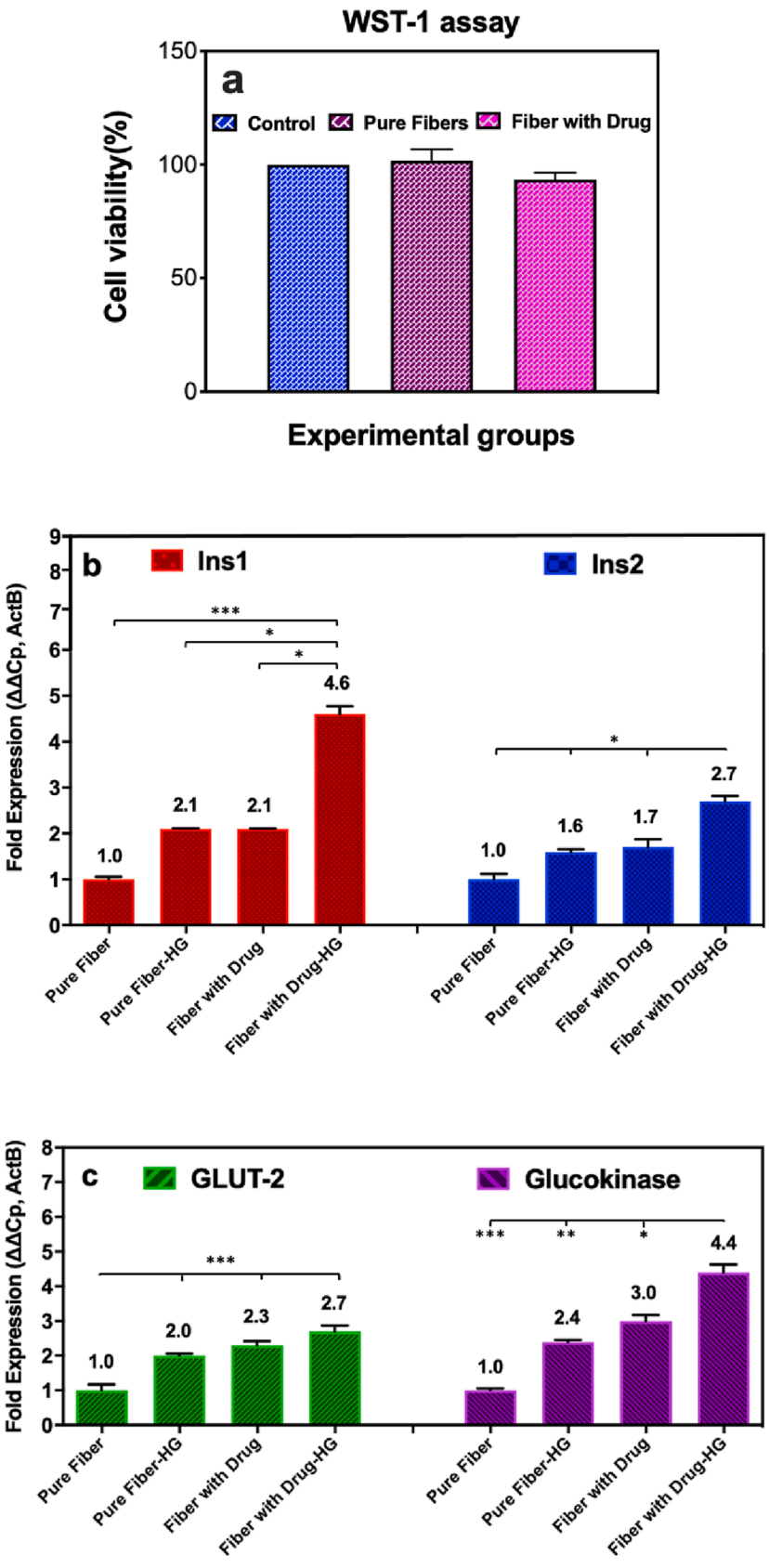

Fig. 5. (a) WST-1 assay of cell viability and (b-c) the expression of insulin, glucokinase, and glucose transporter-2 (GLUT-2) proteins in rat β-cell line, BRIN-BD11. Cells were cultured in the medium with 5.5 mM glucose, pure fiber, EM-loaded fiber, and without fibers. Insulin expression was stimulated by high glucose (25 mM) medium. The expression levels were presented as fold-expression compared with the control cultures. ActB was used as the housekeeping gene. Data represent the mean ± standard error of the mean (n = 3). Significance differences were found at *** $p < 0.001$, ** $p < 0.01$, * $p < 0.05$ between groups. HG: High glucose.

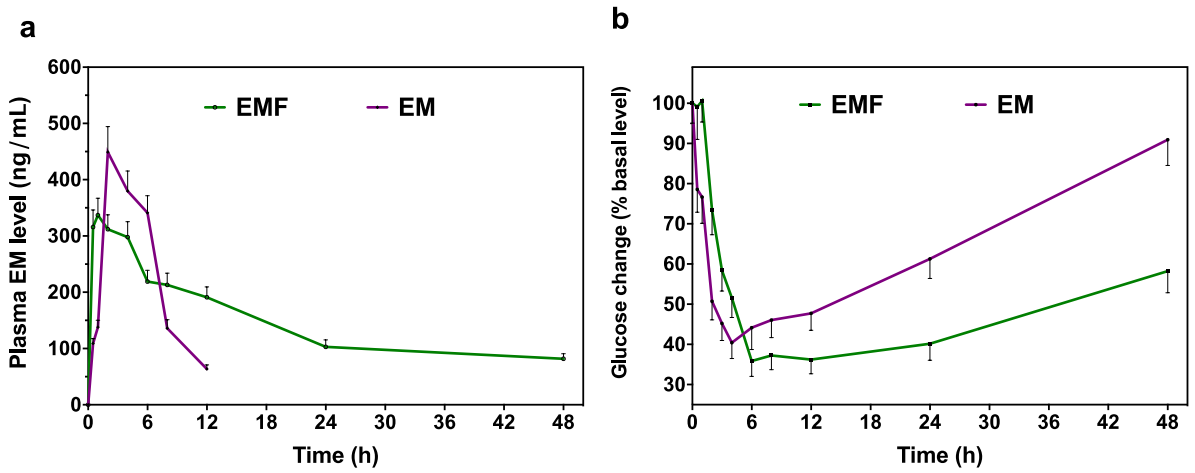

Fig. 6. (a) Plasma EM levels vs. time profiles and (b) BGL of the EM and EMF groups in STZ/NA-induced type 2 diabetic rats. Each group (n = 4) represents mean ± standard error of the mean. (EM: EM-powder given group, EMF: Empagliflozin-loaded three-layer fiber given group, and BGL: Blood glucose levels).

Table 4
Pharmacokinetic parameters of EMF in type 2 diabetic rats.

	EM-powder	EMF
Dose (mg/kg)	10	5
Cmax (ng/mL)	449	337
Tmax (h)	2	1
AUC (μg/mL)	2.8 ± 0.3	6.9 ± 0.8
BA_R (%)	100.0	476 ± 33

Maximum plasma concentration (Cmax), the time to maximum concentration (Tmax), the area under the curve (AUC), and bioavailability (BAR %).

structure of PCL/PLA/PMMA nanofiber. It was proved that EMF in a half dosage compared to EM-powder demonstrated higher bioavailability and EMF can be used in the antidiabetic activity test in the half dosage of EM-powder.

The EM group revealed a higher Cmax (449 ng/mL) and tmax (2 h) than the EMF group, which has a Cmax at 337 ng/mL and tmax at 1 h. There is a rapid increase in the amount of EM in the EM group in 2 h (43% of the total amount) and then, there is a sharp decrease after 6 h. It decreased from 341 to 136 ng/mL from the 6th h till the 8th h. In contrast, although there is a rapid increase in 1 h (32% of the total amount) in the EMF group, the amount of EM gradually decreased in the blood samples of the EMF group. EM could not be detected in the EM group after 12 h. Nevertheless, the amounts of EM were detected as 103 and 82 ng/mL after 24 and 48 h, respectively. As a result, 4% of the total amount was released between 24 and 48 h and this result was matched with the *in vitro* drug release test in which 3% of the total amount was released in this period. The AUC levels and BA_R belonging to the EMF group were ~ 2.5-fold (6.9 ± 0.8 vs. 2.8 ± 0.3 μg/mL) and ~ 4.8-fold (476 ± 33 vs. 100%) higher compared with the EM group, respectively.

3.14. Antidiabetic activity test

3.14.0.1. Body weight

Animals of the same weight range (225–250 g) were used in the experiment. The body weight of the DM group decreased by almost 7% in 3 weeks as a result of muscle wasting and catabolism of tissue proteins, which are the characteristic features of T2DM and causing body weight loss in diabetic rats. Oral administration of EM-powder provided the body weight of the rats to be maintained for 3 weeks. However, EMF provided the body weight not to be changed for 2 weeks but 6% body weight loss was observed between 2 and 3 weeks. As a result, the body weight of the DM group slightly decreased compared with the group C on week 3 ($p < 0.05$) (Fig. 7a). Except for that, there is no significant difference between groups for 3 weeks.

3.14.1. Blood glucose levels.

Fig. 7b demonstrates the alterations in BGL of the rats in all groups for 3 weeks. The BGL of group C was almost 90 mg/dl for 3 weeks and it is within the normal glycemic range for rats. When the rats were divided into 3 groups after inducing T2DM, it is clearly seen that there is no significant difference between them. As expected, group C has the lowest BGL in the beginning (89.7 ± 3.7 mg/dl). In the first week, the BGL of the DM group increased to 425.5 ± 14.2 mg/dl. However, the BGLs of the DM + EM and DM + EMF groups significantly decreased ($p < 0.001$) to 122.2 ± 7.2 and 129.2 ± 13.7 mg/dl in a week. In the second week, the BGLs of group DM + EM were kept constant but they continued to decrease in group DM + EMF (100.3 ± 3.4 mg/dl). Before the decapitation of rats, the BGLs were measured as 94.0 ± 3.9 mg/dl, 427.0 ± 9.0, 99.8 ± 4.6, and 75.5 ± 6.0 mg/dl for groups C, DM, DM + EM, and DM + EMF. As a result, EM treatments in powder and fiber form provided a strong blood glucose-lowering effect but EM-loaded core-sheath fibers supplied similar effects in the half-dosage of EM-powder.

3.14.2. Oral glucose tolerance test (OGTT).

To compare the effect of EM-powder and EM-loaded core-sheath fiber on glucose tolerance, OGTT was applied to rats after 12 h fasting (Fig. 7c). As the usual process in OGTT, treatments were carried out in all groups and a single dose of glucose (2 g/kg, b.w.) was applied 30 min later. The time that glucose was given to rats has been accepted as time 0 and BGLs were started to be measured for 120 min. The slope of the curve of BGL was significantly higher in the diabetic rats than in treated and healthy rats during the first 30 min but an important increase in BGL in this time range was observed and it is verifying the induction of hyperglycemia. The effect of both EM-powder and EMF started on time 0 but EMF prevented the increase of BGL stronger than EM-powder as it is clearly seen from the slope of the curves between 0 and 30 min. In addition, it was shown in the *in vitro* drug release study that 42.8% of all the drug core-sheath fiber contained released within the first 30 min. It can be the reason for fiber preventing the increase of BGL more potent than the powder form. The BGL of the healthy and diabetic rats continued to increase by between 30 and 60 min by 21.8% and 26.7%, respectively. Group DM + EM demonstrated a slight increase by 3.7% and the only treatment that showed a slight decrease in BGL by 30 min was EMF. The BGL of the group DM + EMF continued to decrease in a similar trend and reached 95.0 ± 6.3 mg/dl, which is lower than its beginning BGL (106.3 ± 15.3 mg/dl). Groups C and DM + EM showed similar trends between 60 and 120 min. It can be interpreted that treatment groups and healthy rats tolerated BGL very well but the group DM + EMF showed better and

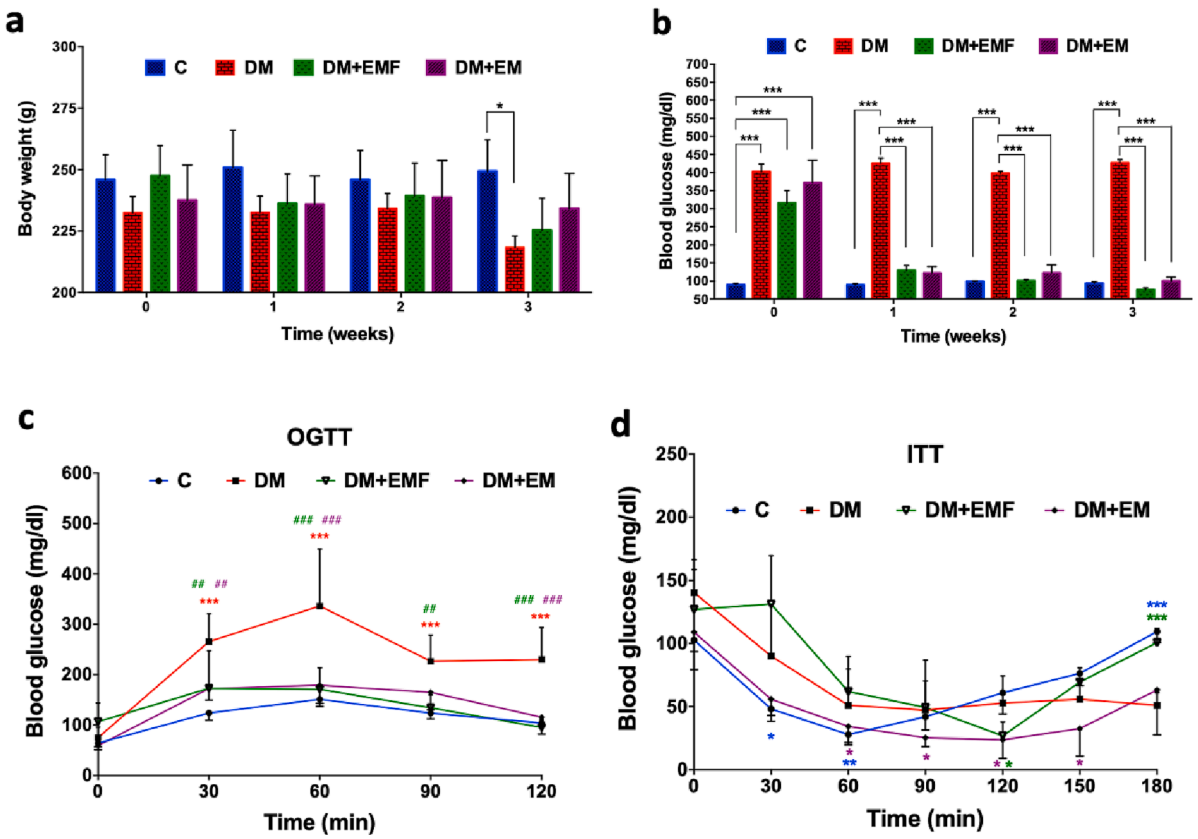

Fig. 7. (a) Body weight and (b) BGL of rats in a period of 3 weeks, (c) oral glucose tolerance test, and (d) insulin tolerance test in rats. Each group (n = 6) represents the mean ± standard error of the mean. *p < 0.05, **p < 0.01, ***p < 0.001 in comparison with diabetes group. (C: Control group, DM: Diabetes group, DM + EMF: Empagliflozin-loaded three-layer fiber treatment group, DM + EM: Empagliflozin-powder treatment group, and BGL: Blood glucose levels).

faster glucose tolerance than the group DM + EM.

3.14.3. Insulin tolerance test (ITT). To evaluate the insulin sensitivity of all groups, 1 U/ kg (i.p.) insulin was applied to rats after 12 h of fasting, and BGL was measured just before the injection and 30, 60, 90, 120, 150, and 180 min after the injection. Ideal insulin tolerance was observed in group C and BGL was completely tolerated in 180 min. The BGL of group C was 102.7 ± 3.8 mg/dl in the beginning and significantly decreased for 60 min, and then it was well tolerated and reached 109.5 ± 3.6 mg/dl in 180 min. Whereas, the BGL of the group DM was not tolerated and it decreased from 140.3 ± 10.6 to 51.0 ± 4.1 mg/dl in 180 min. It is clearly seen from the slope of the curve belonging to the groups DM + EMF and DM + EMF, the BGL of these groups decreased for 120 min and their BGL was similar in 120 min. Later on, their BGL started to increase but the group DM + EMF (100.7 ± 4.3 mg/dl) tolerated it better and faster than the group DM + EM (63.3 ± 13.5 mg/dl) in 180 min (Fig. 7d).

3.15. Biochemical analysis

According to the results of biochemical analysis, the glucagon-like peptide 1 (GLP-1) levels decreased to 384.0 ± 12.2 and 293.5 ± 7.6 ng/g in pancreas and ileum of the group DM compared to the group C (628.5 ± 12.3 and 453.0 ± 22.2 ng/g, respectively). In the both tissues for GLP-1, significant increases were observed in the EMF and EM treatment groups ($p < 0.001$ and $p < 0.01$, respectively) compared to the group DM (Fig. 8a). GLUT-2 levels increased from 19.5 ± 1.5 ng/g to 25.3 ± 0.9 ng/g in the ileums of the group DM. In contrast, GLUT-2 levels decreased from 11.3 ± 0.7 to 7.3 ± 0.3 in the group DM compared to the group C. It was seen that GLUT-2 levels were improved with EMF and EM treatments (13.1 ± 0.8 and 11.9 ± 0.7 ng/g; 17.9 ± 0.4 and 18.7 ± 0.4 ng/g in the pancreas and ileum, respectively) (Fig. 8b).

The peroxisome proliferator-activated receptors gamma (PPAR-γ) levels in the EMF treatment group were almost the same as those of the C group (7.1 ± 0.2 ng/g) in pancreas while this level was 10.7 ± 0.5 ng/g in the EM treatment group. There is no significant difference between groups in the level of PPAR-γ in the ileum (Fig. 8c). On the other hand, a significant increase ($p < 0.001$) was obtained in the sodium-glucose cotransporters-2 (SGLT-2) levels of DM group compared with the C group, while a decrease ($p < 0.001$) was seen in the EMF treatment group compared with the DM group. Furthermore, the levels of SGLT-2 belonging to the EMF treatment group in the pancreas and kidney (9.0 ± 0.4 and 10.1 ± 0.6 ng/g, respectively) were lower than in those of the EM treatment group (12.0 ± 0.4 and 14.8 ± 0.5 ng/g, respectively) (Fig. 8d).

The insulin levels of group C were 6.1 ± 0.1 mIU/g and 14.3 ± 0.3 mIU/L in the pancreas and serum, respectively. In the pancreas, the insulin level of the EMF treatment group (6.2 ± 0.2 mIU/g) was similar to the group C and also, the amount of insulin in the EMF (13.4 ± 0.3 mIU/L) group almost reached those of the group C in serum. EMF treatment succeeded to recover insulin to the condition of healthy rats. (Fig. 8e). The level of tumor necrosis factor-alpha (TNF-α) was found to be increased in the pancreas of the group DM (193.7 ± 14.9 ng/g), EMF (149.0 ± 3.4 ng/g), and EM treatment groups (158.8 ± 2.9 ng/g) compared to the group C (123.30 ± 2.8 ng/g). It was also observed that there was a significant decrease ($p < 0.01$) in the EMF treatment group compared to the group DM. There was no significant difference between the EMF and EM treatment groups. Our results showed that EMF recovered inflammation in the body (Fig. 8f).

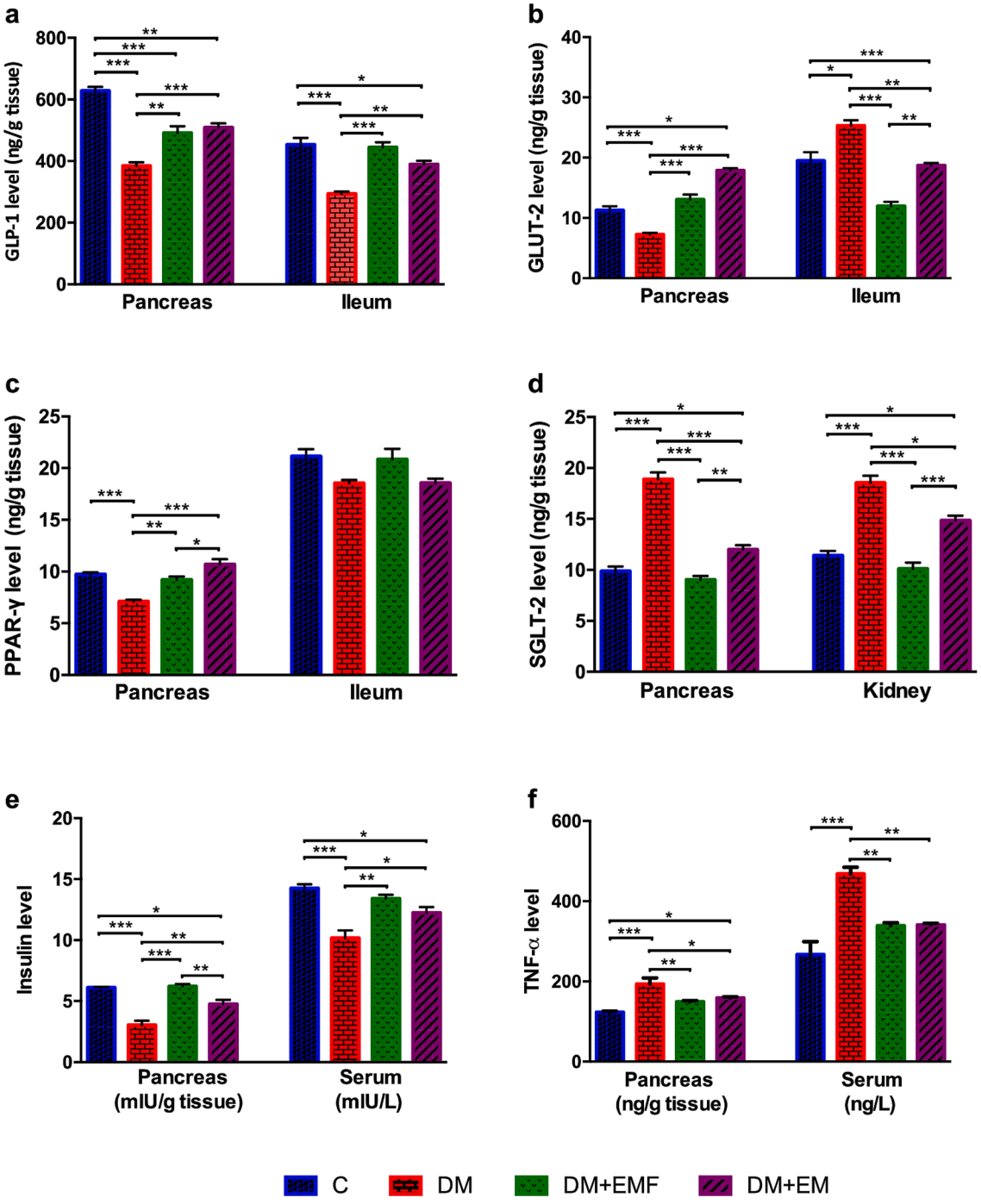

Fig. 8. Effects of EMF and EM-powder (EM) treatments on biochemical parameters in the pancreas, ileum, kidney, and serum. a) GLP-1, b) GLUT-2, c) PPAR-γ, d) SGLT-2, e) Insulin, and f) TNF-α levels. Each group (n = 6) represents the mean ± standard error of the mean. * $p < 0.05$, ** $p < 0.01$, *** $p < 0.001$ in comparison with each other. (C: Control group, DM: Diabetes group, DM + EMF: Empagliflozin-loaded three-layer fiber treatment group, DM + EM: Empagliflozin-powder treatment group).

3.16. Islet β-cell morphology and structural changes

Cellular damage was observed in the liver, pancreas, and kidney tissues of diabetic animals compared with the C group. In the DM group, liver morphology was characterized by severe activation of Kupffer cells, degenerated hepatocytes, and growth of sinusoids. The treatment with EM-powder and EMF provided the regeneration of the liver parenchyma in diabetic rats. Degeneration in the endocrine area and apoptosis/necrosis together with hypertrophy around the acine were observed in pancreatic injury. The pancreatic morphology of diabetic rats that were treated with EM-powder and EMF was found to be the same as the C group. In kidney morphology, there was degeneration in glomeruli and tubules (both proximal and distal) characterized by tubule enlargement and basement membrane separation. Kidney morphologies of the groups DM + EM and DM + EMF exhibited an almost regular appearance of glomeruli and tubules. Tissue reorganization was observed more prominently in the renal parenchyma of the group DM + EMF compared to the group DM + EM (Fig. 9a).

The pancreatic tissue was stained immunocytochemically, using an antibody to insulin, and the number of positively stained cells decreased,

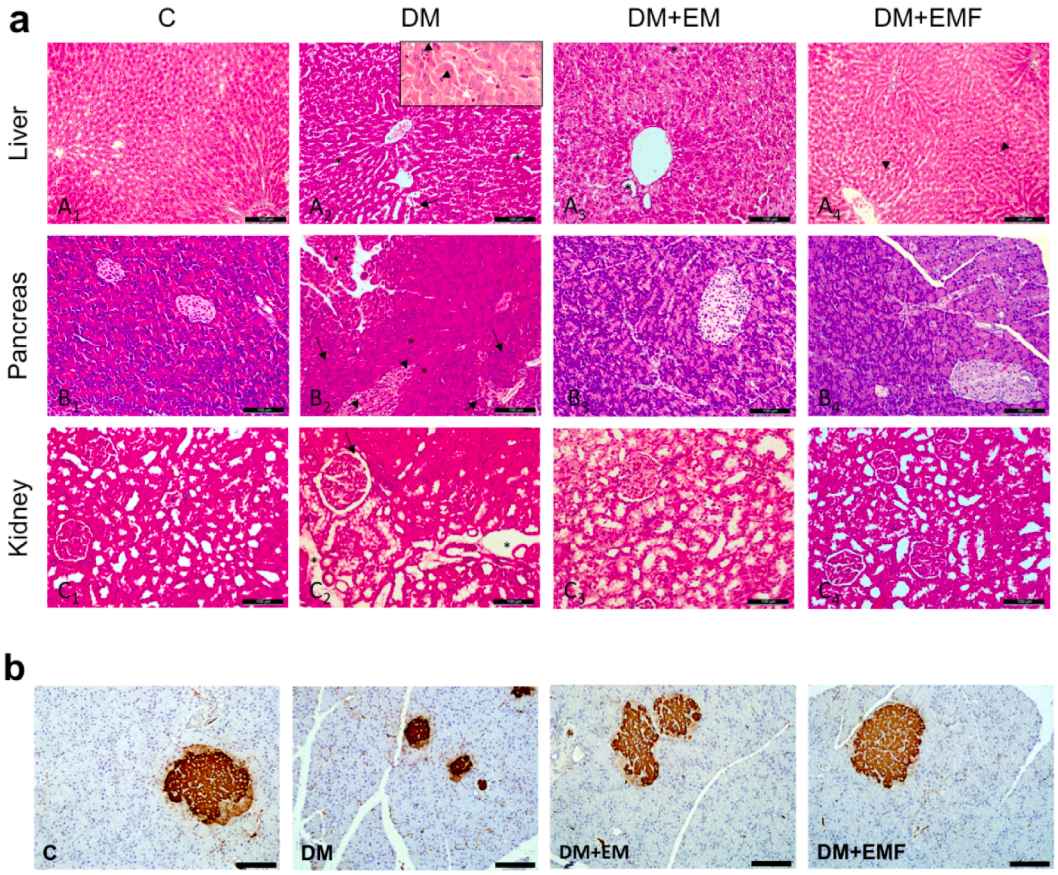

Fig. 9. **(a)** Representative photomicrographs of the liver, pancreas, and kidney tissue in experimental rat groups. Group C: Regular parenchyma morphology of liver, pancreas, and kidney (A1, B1, C1, respectively); Group DM; Increased active Kuppfer cells (arrowhead), dense hemorrhage (black arrow), sinusoidal separations (Asterix), and inflammatory cell infiltration between hepatocytes were observed in the liver tissue (A2). In the pancreatic tissue, degeneration in the endocrine area (arrowhead) and dense apoptotic cells (arrow) together with hypertrophy in the acinar cells (Asterisk) were observed (B2). Tubular enlargement (asterisk) and basement membrane separation (arrow) were seen in the kidney tissue (C2). Groups DM + EM and DM + EMF: Partly active Kuppfer cells (arrowhead) and mild sinusoidal separations (Asterisk) were observed in the liver of both treatment groups (A3,4). In both applications of empagliflozin in pancreatic tissue, a fairly regular acin periphery and endocrine regeneration were observed (B3,4). Similar morphology to the control was observed in the kidney tissue (C3,4). Hematoxylin & Eosin staining; scale bar: 100 μm; insert: 50 μm. (b) Immunohistochemical staining for insulin-positive cells (brown color) in the pancreatic islets of rats in the experimental groups. Scale bar: 100 μm. (C: Control group, DM: Diabetes group, DM + EM: Empagliflozin-powder treatment group, and DM + EMF: Empagliflozin-loaded three-layer fiber treatment group).

hence, insulin staining was decreased in the DM group compared with the C group. It demonstrates that pancreatic β-cells were damaged after the establishment of the animal model (Fig. 9b). An intense insulin staining was detected in the C group, however, this intensity was decreased in the DM group. With EM and EMF treatments, the intensity in the islets was improved similar to the C group and it is showing that treatments were successful in protecting pancreatic β-cells.

4. Discussion

SGLT-2 inhibitors show their effect by decreasing the reabsorption of glucose from the kidneys and increasing the excretion of urine glucose (Nauck, 2014). One of the advantages of SGLT-2 inhibitors is their original mechanism of action independent of insulin. Nevertheless, it is expected that SGLT-2 inhibitors increase glycosuria due to their functions as osmotic diuretics. The improved glucose control and arterial blood pressure, and reduced body weight by using SGLT-2 inhibitors provide positive effects on cardiovascular risk factors. SGLT-2 inhibitors can be used as a monotherapy in diet-treated patients or in combination with another glucose-lowering agent due to their low drug-drug interactions (Fioretto et al., 2016; Scheen, 2015). Therefore, EM, which is one of the most selective SGLT-2 inhibitors, was chosen due to its many advantages mentioned above.

Oral administration is the most preferable drug administration route among all routes due to its features such as easy-to-apply, high patient compliance, low immune system response, no special training for drug utilization, and being painless and economical. Besides these advantages, it is expected to encounter also some disadvantages such as the effects of gastric pH, enzymatic degradation, physiological obstacles, first-pass effect, and late-onset of action in case of using this drug administration route.

Nanofibers have several different advantages such as having small size and high surface area, reducing the frequency of dosage and toxicity, increasing bioavailability, overcoming pharmacokinetic and pharmacodynamic limitations, controlling the drug release, and improving the efficiency of drug delivery system (Ghosh et al., 2019; Kermanizadeh et al., 2018; Kesharwani et al., 2018). Therefore, hydrophobic polymers were used to provide the controlled release of the drug. The release time of EM was prolonged by increasing the number of layers, hence the frequency of drug dosage was reduced and the body was protected against undesirable effects. Furthermore, EM was protected from the high electrical field and denaturation during the fiber production process of tES by loading in the inner layer of produced PCL/PLA/PMMA tri-layer nanofiber. Besides, the pharmacological properties

of EM were protected from the acidic environment of the stomach and degradation in the gastrointestinal system by loading in nanofiber. Also, it provides the controlled and sustained release of the drug, thus reducing the frequency of drug dosage, improving patient compliance, and increasing the bioavailability of the drug compared to the EM powder form. Furthermore, the drug release test demonstrated that 97% of empagliflozin was released in 24 h. If we make only two-layer it would be released faster and we need to repeat the dose for the second time in 24 h, but our target is giving the drug once daily. Consequently, having more layers provides excellent protection, an extended half-life, and increased degradation time according to the results from pharmacokinetic and degradation tests (Ghoroghchian et al., 2006; Ghosh et al., 2019; Hrkach et al., 1996; Kermanizadeh et al., 2018; Shimko and Nauman, 2007; Sperling et al., 2016; Tang et al., 2005).

In this study, all combinations of the tES parameters were tested to determine the optimized parameters by SEM with regard to the morphological structure and diameters of the core-sheath fibers. It was proven that all polymers and EM were successfully loaded in core-sheath nanofibers according to the results of FTIR and XRD tests. On the other hand, fiber diameters were found to be increased after loading EM in core-sheath fibers. Meanwhile, tensile strength and strain at break declined with the addition of EM in fibers. According to the stress–strain curve, the structure of pure fiber was stronger and more flexible than EMF. It was found compatible with the literature that tensile strength decreased with the increase of fiber diameter (Cam et al., 2021; Huang and Young, 2019; Nair et al., 2001; Wong et al., 2008). In addition, a decrease in the Tm and Tg values was observed after EM loading in the DSC test (Alenezi et al., 2019; Wong et al., 2008). The reason for this decrease is thought to be due to physical or chemical interactions between EM and polymers or the crystal structure of EM. On the other hand, the nanofibers that have thinner diameters degrade faster due to larger surface area (Shao et al., 2011). In addition, an increase in swelling ratios by the addition of EM in nanofibers was observed due to the hydroxyl groups of EM and increased fiber diameters (Entekhabi et al., 2016).

According to the results of the drug release test, it was seen that 97% of all drug contained in fibers was released in a controlled manner at the end of 24 h as intended, while 42.78% of this release was performed as to be a burst release in the first 30 min. There is no negative influence of the crystal state of EM on drug release. In addition, EM was loaded in the fibers successfully with a very high EE value. Although half of the EM-powder treatment dosage used for rats was loaded in the fibers, the results of animal tests proved that fiber treatment is more successful than the powder form, which is the currently used dosage form for EM. Thus, it was tried to create a new treatment strategy that has better antidiabetic effects and fewer side effects using core-sheath nanofibers.

The cell viability maintained at the same as equal as the group C since the fiber materials have no effects on cells negatively. On the other hand, the cells cultured on EMF showed moderate loss of cell viability after 48 h, nevertheless, the percentage of the cell viability was above the threshold value of 70%. According to ISO 10993–5, the test item is considered to be non-cytotoxic if the percentage of viability is equal to or greater than 70% of the group C (ISO 2009). Therefore, the produced new nanotechnological product could be considered to be well-suited due to their effects on cell viability for clinical application.

The use of EMF in the cell culture substantially improved the β-cell function due to its EM content (Al Jobori et al., 2018). Both GLUT-2 and pancreatic isoform of glucokinase was shown to be a part of the peripheral glucose-sensing mechanism in β-cells for the detection of the increased BGL that are an obstacle to maintaining a proper homeostasis (Uranga et al., 2017). The expression of GLUT-2 and glucokinase proteins was considerably increased after the EMF treatment and the expression of insulin was improved by these fibers. The ratio of insulin expression at high glucose levels compared to low glucose levels remained unchanged during the treatment with EM. The expression levels of GLUT-2 and glucokinase increased by more than 2 times due to the induction effect of EM, also, this situation might be led to an increase in the expressed level of insulin in the β-cells.

In the studies using hydrophobic polymers such as PLA, PCL, and PMMA, bioavailability has been improved (Nie et al., 2020). In a study, bioavailability has been increased 3.6-fold in a micelle formulation prepared with PLA in rats (Mu et al., 2010). A significant increase in the oral bioavailability has been found for didehydroandrographolide-loaded PCL nanoparticles, which was 10.8-fold higher than the free DDA and demonstrated a slow and sustained drug release from the polymer matrix in STZ/NA-induced diabetic rats (Nagalakshmi, K., Sujatha, S., Alwin, D., 2017). In the current study, the bioavailability was improved by ~ 4.8-fold by loading EM to tri-layer PCL/PLA/PMMA fibers compared to EM-powder. In order to improve EM bioavailability by producing a tri-layer nanofiber is an unprecedented and promotive treatment approach according to the results of the pharmacokinetic test applied on rats.

It is known that muscle loss and catabolism of tissue proteins cause the decrease in body weight seen in the T2DM group (Cam et al., 2017; Kheiripour et al., 2019). In previous studies, EM treatment has been reported to reduce weight gain in rats even in the case of there being more food intake compared to untreated rats (Assaly et al., 2018). Also, fluid loss due to the osmotic diuresis effect of EM may contribute to a faster weight reduction by the beginning of treatment. It is thought that EM treatment slightly decreased muscle loss and catabolism of tissue proteins caused by STZ/NA, and urinary glucose excretion caused by weight loss. In our study, there was no difference between the EM and EMF treatment groups in the change of body weight.

In addition, the high BGL seen in diabetes was decreased by using the EM and EMF treatments. There is no difference in BGLs between the EM and EMF treatment groups. It has been shown in previous studies that BGL was successfully reduced in rats with EM treatments administered at a dose of 10 mg/kg (Steven et al., 2017). In our study, the same success was achieved with 5 mg/kg of EMF. The reason for the decrease in BGL is due to the fact that EM provides glucose excretion with urinary excretion (Frampton, 2018). Furthermore, in all groups, a decrease in BGL was observed initially due to the effects of insulin in ITT. The decrease in both the EM and EMF treatment groups continued up to 120 min, and after 120 min, the glucose level increased sharply according to the results of ITT. It can be seen that EMF tolerated BGL more successfully than EM treatment.

According to the OGTT, the results of the EM and EMF groups were found similar to the results of the T2DM group, only EMF treatment seemed to be more successful in decreasing glucose compared to EM treatment at 90th min measurement. Successful blood glucose-lowering effect in the treatment groups shows that EM enhances the delayed insulin response seen in diabetes, inhibits glucose reabsorption in the kidney to control glucose levels without hypoglycaemic side effects, provides weight loss, and therefore increases the usability of glucose by cells (Cam et al., 2017; Park et al., 2019). These effects of EM are thought to be due to increased insulin sensitivity, reversing glucotoxicity, and normalizing glucose homeostasis in T2DM, apart from the main mechanism of action (Cheng et al., 2016).

In this study, the level of GLP-1, GLUT-2, PPAR-γ, SGLT-2, insulin, and TNF-α were evaluated in different tissues for the determination of their effects on glucose metabolism in the human body. Thus, the GLP-1 receptor agonist prevents T2DM since provides lowered body weight and hyperglycemia (Moritoh et al., 2010; Tornehave et al., 2008; Xu et al., 2006). In our study, the EMF treatment group provided an increase in GLP-1 in diabetic rats. GLUT-2 provides higher glucose to transfer into β-cells and the reduction of GLUT-2 levels has resulted in the onset of DM (Amalan et al., 2016; Arya et al., 2012). The GLUT-2 levels were increased in the pancreas and reduced in the ileum by EMF treatment in this study. In addition, PPAR-γ has effects on glucose and lipid metabolism as a regulator and it is also contributed to the improvement of response to T2DM and insulin resistance by these effects (Fiévet et al., 2006; PAHEL et al., 2004). In our study, PPAR-γ and

insulin levels of the C group were almost the same as those of the EMF treatment group. On the other hand, SGLT-2 has a crucial role in glucose reabsorption from the proximal tubules of the kidney. The excretion of glucose in the urine is increased in the treatment of T2DM by using SGLT-2 inhibitors (Grempler et al., 2012; Kojima et al., 2015). TNF-α, which is a proinflammatory cytokine, has significant regulatory functions in carbohydrate and protein metabolism, and insulin resistance (Pedersen et al., 2003; Stewart et al., 2001). As a result of this study, SGLT-2 and TNF-α levels in the DM group increased while a significant decrease in these parameters was observed in the EMF treatment group. Thus, it was proven that the EMF treatment group has anti-diabetic effects in this study.

In diabetes condition, severe activation of Kupffer cells, degenerated hepatocytes, and growth of sinusoids in the liver; degeneration in the endocrine area and apoptosis/necrosis together with hypertrophy around the acine in the pancreas; and degeneration in glomeruli and tubules (both proximal and distal) characterized by tubule enlargement and basement membrane separation in the kidney are observed (Miller and Zachary, 2017). The cellular damage in the liver, pancreas, and kidney tissues was improved with EM and EMF treatments.

Chronic increase in BGL (i.e., glucotoxicity) impairs β-cell function. In contrast, it was proved in both *in vitro* and *in vivo* studies that reducing BGL improves insulin secretion (Al Jobori et al., 2018). SGLT-2 inhibitors such as dapagliflozin and EM reduce or normalize BGL and improve β-cell function in preclinical studies of diabetic animal models (Ferrannini et al., 2014; Merovci et al., 2015). In a study conducted by Cheng et al., it has been indicated that β-cell area/total pancreatic area and Ki-67 (co-stained with insulin) expression, which is a cell proliferation marker, were significantly increased with EM treatment according to the immunohistochemical analysis (Cheng et al., 2016). In another study, it has been shown that EM protected diabetic pancreatic cells by inhibiting the activation of the nucleotide-binding oligomerization domain-like receptor protein 3/caspase-1/ Gasdermin D pathway in pancreatic β cells according to the results of *in vitro* and *in vivo* studies (Liu et al., 2021). In the immunohistochemical assessment of the insulin content in pancreatic β-cells of the current study, although there is a decrease in the intensity of type 2 diabetic islets in rats, the number of positively stained cells was increased with EM and EMF treatments.

Consequently, as a result of all these completed tests, it was proved that half of the EM-powder dosage used for rats was successfully loaded in tri-layer PCL/PLA/PMMA fibers. It was also shown that EMF with its serious advantages effectively treated T2DM by the oral route.

5. Conclusion

Oral tri-layer EM-loaded PCL/PLA/PMMA fibers were successfully produced by using tES for the treatment of T2DM. The anti-diabetic effects of these core-sheath fibers were compared with EM-powder dosage form by *in vivo* animal and *in vitro* cell culture tests. Tensile strength, Tm, and Tg values decreased by adding EM in fiber. The 97% of all drug contained in fibers was released in a controlled manner at the end of 24 h as intended. Thus, the frequency of dosage was reduced due to the sustained release of EM. The cell viability in the rat β-cell line (BRIN-BD11) was maintained by both EMF and pure fibers. The expressions of glucokinase and GLUT-2 that are relevant for the glucose-sensing mechanism increased due to the effect of EM. The induction of expression for these proteins provided to increase in the expression of Ins1 and Ins2. The bioavailability was enhanced ~4.8-fold with the EMF treatment compared to EM-powder and BGL was controlled for 48 h with EMF. Furthermore, oral EMF demonstrated better sustainable anti-diabetic activity even in the half dosage than EM-powder dosage form by providing a significant decrease in body weight and BGL, improvements in glucose tolerance, and insulin sensitivity of STZ/NA-induced T2DM rats. While the levels of GLP-1, PPAR-γ, and insulin increased, the levels of SGLT-2, GLUT-2, and TNF-α decreased in comparison with the DM group after EMF treatment. On the other hand, it was proven that the observed cellular damages in the liver, pancreas, and kidney tissues of diabetic animals were improved with EMF treatment according to the histological analysis. Furthermore, in immunohistochemical analysis, pancreatic β-cells were protected and an intense insulin staining was observed with EMF treatment. Consequently, oral administration of tri-layer EMF, which is a promising approach as a new treatment strategy, has a high potential for the treatment of T2DM according to the detailed investigations.

CRediT authorship contribution statement

Ece Guler: Investigation, Methodology, Visualization, Writing – original draft, Writing – review & editing. **Ayse Nur Hazar-Yavuz:** Investigation, Methodology, Visualization, Writing – original draft, Writing – review & editing. **Esra Tatar:** Investigation, Methodology, Writing – original draft. **Mohammad Morid Haidari:** Investigation, Methodology. **Gul Sinemcan Ozcan:** Investigation, Methodology, Writing – original draft. **Gokhan Duruksu:** Investigation, Methodology, Writing – original draft. **Manuel Pedro F Graça:** Writing – review & editing. **Deepak M Kalaskar:** Writing – review & editing. **Oguzhan Gunduz:** Writing – review & editing, Funding acquisition. **Muhammet Emin Cam:** Conceptualization, Validation, Writing – original draft, Supervision, Writing – review & editing, Funding acquisition.

Declaration of Competing Interest

The authors declare that they have no known competing financial interests or personal relationships that could have appeared to influence the work reported in this paper.

Data availability

Data will be made available on request.

Acknowledgments

E.G. and A.N.H-Y. contributed equally to this work. This project was supported by a TUBITAK 2209-A Research Projects Program Grant (2209-A, 2020/2, No: 1919B012002602, Scientific and Technological Research Council of Turkey-TUBITAK). M.E.C. gratefully acknowledges Marmara University, Scientific Research Projects Committee (MU-BAPKO; SAG-K-170118-0001 and SAG-A-110618-0292) and Koç University Surface Science and Technology Center (KUYTAM). M.E.C. would also like to thank Burak Bayram at Koç University for the FIB-SEM analysis and Bilge Tuzcu at Marmara University, Faculty of Pharmacy for drawing the table of contents (TOC). E.G. acknowledges the Council of Higher Education, TUBITAK 2211-A, and TUBITAK 2250 for her scholarships. The authors dedicate this article to the memory of Turkish citizens, who lose their in the earthquake held in Pazarcık and Elbistan, Kahramanmaraş, Türkiye on 6/2/2023.

Appendix A. Supplementary data

Supplementary data to this article can be found online at https://doi.org/10.1016/j.ijpharm.2023.122716.

References

Abdelrazek, E., Hezma, A., El-Khodary, A., Elzayat, A., 2016. Spectroscopic studies and thermal properties of PCL/PMMA biopolymer blend. Egypt. J. Basic Appl. Sci. 3, 10–15.

Aguzzi, C., Cerezo, P., Salcedo, I., Sánchez, R., Viseras, C., 2010. Mathematical models describing drug release from biopolymeric delivery systems. Mater. Technol. 25, 205–211.

Al Jobori, H., Daniele, G., Adams, J., Cersosimo, E., Solis-Herrera, C., Triplitt, C., DeFronzo, R.A., Abdul-Ghani, M., 2018. Empagliflozin Treatment Is Associated With Improved β-Cell Function in Type 2 Diabetes Mellitus. J. Clin. Endocrinol. Metab. 103, 1402–1407.

Alberti, K.G.M.M., Zimmet, P.Z., 1998. Definition, diagnosis and classification of diabetes mellitus and its complications. Part 1: diagnosis and classification of diabetes mellitus. Provisional report of a WHO consultation. Diabet. Med. 15, 539–553.
Alenezi, H., Cam, M.E., Edirisinghe, M., 2019. Experimental and theoretical investigation of the fluid behavior during polymeric fiber formation with and without pressure. Appl. Phys. Rev. 6, 041401.
Alenezi, H., Cam, M.E., Edirisinghe, M., 2021. Core–sheath polymer nanofiber formation by the simultaneous application of rotation and pressure in a novel purpose-designed vessel. Appl. Phys. Rev. 8, 041412.
Alfares, F.S., Guler, E., Alenezi, H., Cam, M.E., Edirisinghe, M., 2021. Optimization of Process-Control Parameters for the Diameter of Electrospun Hydrophilic Polymeric Composite Nanofibers. Macromol. Mater. Eng. 306, 2100471.
Amalan, V., Vijayakumar, N., Indumathi, D., Ramakrishnan, A., 2016. Antidiabetic and antihyperlipidemic activity of p-coumaric acid in diabetic rats, role of pancreatic GLUT 2: In vivo approach. Biomed. Pharmacother. 84, 230–236.
Arya, A., Looi, C.Y., Cheah, S.C., Mustafa, M.R., Mohd, M.A., 2012. Anti-diabetic effects of Centratherum anthelminticum seeds methanolic fraction on pancreatic cells, β-TC6 and its alleviating role in type 2 diabetic rats. J. Ethnopharmacol. 144, 22–32.
Assaly, R., Gorny, D., Compagnie, S., Mayoux, E., Bernabe, J., Alexandre, L., Giuliano, F., Behr-Roussel, D., 2018. The favorable effect of empagliflozin on erectile function in an experimental model of type 2 diabetes. J. Sex. Med. 15, 1224–1234.
Aydin, S., Kabaoglu, I., Guler, E., Topal, F., Hazar-Yavuz, A.N., Ekentok, C., Tatar, E., Gurbuz, F., Gunduz, O., Cam, M.E., 2022. A Comparison Study of Fiber Diameter's Effect on Characteristic Features of Donepezil/Curcumin-Loaded Polycaprolactone/Polylactic Acid Nanofibers. Macromol. Mater. Eng. 307, 2100855.
Badole, S.L., Chaudhari, S.M., Jangam, G.B., Kandhare, A.D., Bodhankar, S.L., 2015. Cardioprotective activity of Pongamia pinnata in streptozotocin-nicotinamide induced diabetic rats. Biomed Res. Int. 2015, 403291.
Barnett, A.H., Mithal, A., Manassie, J., Jones, R., Rattunde, H., Woerle, H.J., Broedl, U.C., 2014. Efficacy and safety of empagliflozin added to existing antidiabetes treatment in patients with type 2 diabetes and chronic kidney disease: a randomised, double-blind, placebo-controlled trial. Lancet Diabetes Endocrinol 2, 369–384.
Bhole, R.P., Tamboli, F.R., 2018. Development and Validation of Stability Indicating HPTLC-MS Method for Estimation of Empagliflozin in Pharmaceutical Dosage Form. Anal. Chem. Lett. 8, 244–256.
Boland, B., Mumphrey, M.B., Hao, Z., Gill, B., Townsend, R.L., Yu, S., Münzberg, H., Morrison, C.D., Trevaskis, J.L., Berthoud, H.-R., 2019. The PYY/Y2R-Deficient Mouse Responds Normally to High-Fat Diet and Gastric Bypass Surgery. Nutrients 11, 585.
Bullard, K.M., Cowie, C.C., Lessem, S.E., Saydah, S.H., Menke, A., Geiss, L.S., Orchard, T. J., Rolka, D.B., Imperatore, G., 2018. Prevalence of diagnosed diabetes in adults by diabetes type—United States, 2016. MMWR Morb. Mortal. Wkly. 67, 359.
Cam, M.E., Ertas, B., Alenezi, H., Hazar-Yavuz, A.N., Cesur, S., Ozcan, G.S., Ekentok, C., Guler, E., Katsakouli, C., Demirbas, Z., Akakin, D., Eroglu, M.S., Kabasakal, L., Gunduz, O., Edirisinghe, M., 2021. Accelerated diabetic wound healing by topical application of combination oral antidiabetic agents-loaded nanofibrous scaffolds: An in vitro and in vivo evaluation study. Mater. Sci. Eng. C 119, 111586.
Cam, M.E., Hazar-Yavuz, A.N., Yildiz, S., Ertas, B., Adakul, B.A., Taskin, T., Alan, S., Kabasakal, L., 2019. The methanolic extract of Thymus praecox subsp. skorpilii var. skorpilii restores glucose homeostasis, ameliorates insulin resistance and improves pancreatic β-cell function on streptozotocin/nicotinamide-induced type 2 diabetic rats. J. Ethnopharmacol. 231, 29–38.
Cam, M.E., Yildiz, S., Alenezi, H., Cesur, S., Ozcan, G.S., Erdemir, G., Edirisinghe, U., Akakin, D., Kuruca, D.S., Kabasakal, L., Gunduz, O., Edirisinghe, M., 2020. Evaluation of burst release and sustained release of pioglitazone-loaded fibrous mats on diabetic wound healing: an in vitro and in vivo comparison study. J. R. Soc. Interface 17, 20190712.
Cam, M.E., Yildiz, S., Ertas, B., Acar, A.E., Taskin, T., Kabasakal, L., 2017. Antidiabetic effects of Salvia triloba and Thymus praecox subsp. Skorpilii var. skorpilii in a rat model of streptozotocin/nicotinamide-induced diabetes. Marmara Pharm. J. 21, 818–827.
Cheng, S.T.W., Chen, L., Li, S.Y.T., Mayoux, E., Leung, P.S., 2016. The Effects of Empagliflozin, an SGLT2 Inhibitor, on Pancreatic β-Cell Mass and Glucose Homeostasis in Type 1 Diabetes. PLoS One 11, e0147391.
Chew, K., Ng, T., How, Z., 2013. Conductivity and microstructure study of PLA-based polymer electrolyte salted with lithium perchloride, LiClO4. Int. J. Electrochem. Sci. 8.
Çubuk, G., İnce, S., 2015. Oral Antidiyabetik İlaçlar. Kocatepe. Vet. J. 8, 95–102.
DeFronzo, R.A., 1999. Pharmacologic therapy for type 2 diabetes mellitus. Ann. Intern. Med. 131, 281–303.
Devikala, S., Kamaraj, P., Arthanareeswari, M., 2016. Sensing of acetone vapours using polymer composite. Orient. J. Chem. 32, 2269–2274.
Dong, Y., Liao, S., Ngiam, M., Chan, C.K., Ramakrishna, S., 2009. Degradation behaviors of electrospun resorbable polyester nanofibers. Tissue Eng. Part B Rev. 15, 333–351.
Entekhabi, E., Nazarpak, M.H., Moztarzadeh, F., Sadeghi, A., 2016. Design and manufacture of neural tissue engineering scaffolds using hyaluronic acid and polycaprolactone nanofibers with controlled porosity. Mater. Sci. Eng. C 69, 380–387.
Farokhzad, O.C., Langer, R., 2009. Impact of Nanotechnology on Drug Delivery. ACS Nano 3, 16–20.
Ferrannini, E., Muscelli, E., Frascerra, S., Baldi, S., Mari, A., Heise, T., Broedl, U.C., Woerle, H.-J., 2014. Metabolic response to sodium-glucose cotransporter 2 inhibition in type 2 diabetic patients. J. Clin. Investig. 124, 499–508.
Ferriol, M., Gentilhomme, A., Cochez, M., Oget, N., Mieloszynski, J., 2003. Thermal degradation of poly (methyl methacrylate)(PMMA): modelling of DTG and TG curves. Polym. Degrad. Stab. 79, 271–281.
Fiévet, C., Fruchart, J.-C., Staels, B., 2006. PPARα and PPARγ dual agonists for the treatment of type 2 diabetes and the metabolic syndrome. Curr. Opin. Pharmacol. 6, 606–614.
Fioretto, P., Zambon, A., Rossato, M., Busetto, L., Vettor, R., 2016. SGLT2 inhibitors and the diabetic kidney. Diabetes Care 39, S165-S171.
Fonseca, V., Rosenstock, J., Patwardhan, R., Salzman, A., 2000. Effect of metformin and rosiglitazone combination therapy in patients with type 2 diabetes mellitus: a randomized controlled trial. JAMA 283, 1695–1702.
Frampton, J.E., 2018. Empagliflozin: a review in type 2 diabetes. Drugs 78, 1037–1048.
Frenot, A., Chronakis, I.S., 2003. Polymer nanofibers assembled by electrospinning. Curr. Opin. Colloid. Interface Sci. 8, 64–75.
Ghoroghchian, P.P., Li, G., Levine, D.H., Davis, K.P., Bates, F.S., Hammer, D.A., Therien, M.J., 2006. Bioresorbable vesicles formed through spontaneous self-assembly of amphiphilic poly (ethylene oxide)-block-polycaprolactone. Macromolecules 39, 1673–1675.
Ghosh, S., Ghosh, S., Sil, P.C., 2019. Role of nanostructures in improvising oral medicine. Toxicol. Rep. 6, 358–368.
Glovaci, D., Fan, W., Wong, N.D., 2019. Epidemiology of diabetes mellitus and cardiovascular disease. Curr. Cardiol. Rep. 21, 1–8.
Grempler, R., Thomas, L., Eckhardt, M., Himmelsbach, F., Sauer, A., Sharp, D., Bakker, R., Mark, M., Klein, T., Eickelmann, P., 2012. Empagliflozin, a novel selective sodium glucose cotransporter-2 (SGLT-2) inhibitor: characterisation and comparison with other SGLT-2 inhibitors. Diabetes Obes. Metab. 14, 83–90.
Hjelm, K., Mufunda, E., Nambozi, G., Kemp, J., 2003. Preparing nurses to face the pandemic of diabetes mellitus: a literature review. J. Adv. Nurs. 41, 424–434.
Hrkach, J.S., Ou, J., Lotan, N., Langer, R., 1996. Poly (L-Lactic acid-co-amino acid) graft copolymers: A class of functional biodegradable biomaterials. ACS Publications. 8, 93–102.
Huang, J.-K., Young, W.-B., 2019. The mechanical, hygral, and interfacial strength of continuous bamboo fiber reinforced epoxy composites. Compos. B. Eng. 166, 272–283.
Ibrahim, R.K., Hayyan, M., AlSaadi, M.A., Ibrahim, S., Hayyan, A., Hashim, M.A., 2019. Physical properties of ethylene glycol-based deep eutectic solvents. J. Mol. Liq. 276, 794–800.
Imagawa, A., Hanafusa, T., Miyagawa, J.-I., Matsuzawa, Y., 2000. A novel subtype of type 1 diabetes mellitus characterized by a rapid onset and an absence of diabetes-related antibodies. N. Engl. J. Med. 342, 301–307.
Jahromi, L.P., Ghazali, M., Ashrafi, H., Azadi, A., 2020. A comparison of models for the analysis of the kinetics of drug release from PLGA-based nanoparticles. Heliyon 6, e03451.
Javanbakht, S., Nezhad-Mokhtari, P., Shaabani, A., Arsalani, N., Ghorbani, M., 2019. Incorporating Cu-based metal-organic framework/drug nanohybrids into gelatin microsphere for ibuprofen oral delivery. Mater. Sci. Eng. C 96, 302–309.
Jiang, W., Zhang, X., Liu, P., Zhang, Y., Song, W., Yu, D.-G., Lu, X., 2022. Electrospun healthcare nanofibers from medicinal liquor of Phellinus igniarius. Adv. Comp. Hybrid Mater. 5, 3045–3056.
Kaczmarek, H., Nowicki, M., Vuković-Kwiatkowska, I., Nowakowska, S., 2013. Crosslinked blends of poly (lactic acid) and polyacrylates: AFM, DSC and XRD studies. J. Polym. Res. 20, 91.
Kelnar, I., Kratochvíl, J., Fortelny, I., Kaprálková, L., Zhigunov, A., Khunová, V., Nevoralová, M., 2016. Effect of halloysite on structure and properties of melt-drawn PCL/PLA microfibrillar composites. Express Polym. Lett. 10, 381.
Kermanizadeh, A., Powell, L.G., Stone, V., Møller, P., 2018. Nanodelivery systems and stabilized solid-drug nanoparticles for orally administered medicine: current landscape. Int. J. Nanomedicine 13, 7575.
Kesharwani, P., Gorain, B., Low, S.Y., Tan, S.A., Ling, E.C.S., Lim, Y.K., Chin, C.M., Lee, P.Y., Lee, C.M., Ooi, C.H., 2018. Nanotechnology based approaches for anti-diabetic drugs delivery. Diabetes Res. Clin. Pract. 136, 52–77.
Khan, M.S., Qazi, R.A., Wahid, M.S., 2008. Miscibility studies of PVC/PMMA and PS/PMMA blends by dilute solution viscometry and FTIR. Afr. J. Pure Appl. Chem. 2, 041–045.
Khatiwala, V.K., Shekhar, N., Aggarwal, S., Mandal, U., 2008. Biodegradation of poly (ε-caprolactone)(PCL) film by Alcaligenes faecalis. J. Polym. Environ. 16, 61–67.
Kheiripour, N., Karimi, J., Khodadadi, I., Tavilani, H., Goodarzi, M.T., Hashemnia, M., 2019. Hepatoprotective effects of silymarin on liver injury via irisin upregulation and oxidative stress reduction in rats with type 2 diabetes. Iran. J. Med. Sci. 44, 108.
Kojima, N., Williams, J.M., Slaughter, T.N., Kato, S., Takahashi, T., Miyata, N., Roman, R. J., 2015. Renoprotective effects of combined SGLT 2 and ACE inhibitor therapy in diabetic D ahl S rats. Physiol. Rep. 3, e12436.
Lee, W.F., Fu, Y.T., 2003. Effect of montmorillonite on the swelling behavior and drug-release behavior of nanocomposite hydrogels. J. Appl. Polym. Sci. 89, 3652–3660.
Liu, F., Vyas, C., Poologasundarampillai, G., Pape, I., Hinduja, S., Mirihanage, W., Bartolo, P., 2018. Structural evolution of PCL during melt extrusion 3D printing. Macromol. Mater. Eng. 303, 1700494.
Liu, H., Jiang, W., Yang, Z., Chen, X., Yu, D.-G., Shao, J., 2022a. Hybrid films prepared from a combination of electrospinning and casting for offering a dual-phase drug release. Polymers 14, 2132.
Liu, H., Wang, H., Lu, X., Murugadoss, V., Huang, M., Yang, H., Wan, F., Yu, D.-G., Guo, Z., 2022b. Electrospun structural nanohybrids combining three composites for fast helicide delivery. Adv. Comp. Hybrid Mater. 1–13.
Liu, L., Bai, S., Yang, H., Li, S., Quan, J., Zhu, L., Nie, H., 2016. Controlled release from thermo-sensitive PNVCL-co-MAA electrospun nanofibers: The effects of hydrophilicity/hydrophobicity of a drug. Mater. Sci. Eng. C 67, 581–589.

Liu, P., Zhang, Z., Wang, J., Zhang, X., Yu, X., Li, Y., 2021. Empagliflozin protects diabetic pancreatic tissue from damage by inhibiting the activation of the NLRP3/caspase-1/GSDMD pathway in pancreatic β cells: in vitro and in vivo studies. Bioengineered 12, 9356–9366.
Liu, Y., Chen, X., Gao, Y., Yu, D.-G., Liu, P., 2022c. Elaborate design of shell component for manipulating the sustained release behavior from core–shell nanofibres. J. Nanobiotechnology 20, 1–17.
Mangin, R., Vahabi, H., Sonnier, R., Chivas-Joly, C., Lopez-Cuesta, J.-M., Cochez, M., 2020. Assessment of the protective effect of PMMA on water immersion ageing of flame retarded PLA/PMMA blends. Polym. Degrad. Stab. 174, 109104.
Martin, A., Cai, J., Schaedel, A.-L., van der Plas, M., Malmsten, M., Rades, T., Heinz, A., 2022. Zein-polycaprolactone core–shell nanofibers for wound healing. Int. J. Pharm. 621, 121809.
Mathers, C.D., Loncar, D., 2006. Projections of global mortality and burden of disease from 2002 to 2030. PloS Med 3, e442.
Meng, Z., Zheng, W., Li, L., Zheng, Y., 2010. Fabrication and characterization of three-dimensional nanofiber membrance of PCL–MWCNTs by electrospinning. Mater. Sci. Eng. C 30, 1014–1021.
Merovci, A., Mari, A., Solis, C., Xiong, J., Daniele, G., Chavez-Velazquez, A., Tripathy, D., Urban McCarthy, S., Abdul-Ghani, M., DeFronzo, R.A., 2015. Dapagliflozin lowers plasma glucose concentration and improves β-cell function. J. Clin. Endocrinol. Metab. 100, 1927–1932.
Michel, M.C., Mayoux, E., Vallon, V., 2015. A comprehensive review of the pharmacodynamics of the SGLT2 inhibitor empagliflozin in animals and humans. Naunyn Schmiedebergs Arch Pharmacol. 388, 801–816.
Miller, M.A., Zachary, J.F., 2017. Mechanisms and Morphology of Cellular Injury, Adaptation, and Death. Pathologic Basis of Veterinary Disease 2–43, e19.
Mishra, N., Tiwari, V.K., Schmidt, R.R., 2020. Recent trends and challenges on carbohydrate-based molecular scaffolding: general consideration toward impact of carbohydrates in drug discovery and development. Carbohydrates in Drug Discovery and Development 1–69.
Modi, P., 2007. Diabetes beyond insulin: review of new drugs for treatment of diabetes mellitus. Curr. Drug Discov. Technol. 4, 39–47.
Moritoh, Y., Takeuchi, K., Hazama, M., 2010. Combination treatment with alogliptin and voglibose increases active GLP-1 circulation, prevents the development of diabetes and preserves pancreatic beta-cells in prediabetic db/db mice. Diabetes Obes. Metab. 12, 224–233.
Mu, C.-F., Balakrishnan, P., Cui, F.-D., Yin, Y.-M., Lee, Y.-B., Choi, H.-G., Yong, C.S., Chung, S.-J., Shim, C.-K., Kim, D.-D., 2010. The effects of mixed MPEG–PLA/Pluronic® copolymer micelles on the bioavailability and multidrug resistance of docetaxel. Biomaterials 31, 2371–2379.
ISO 10993-5:2009, 2009. Biological evaluation of medical devices. Part 1, 10993.
Nair, R., Nyamweya, N., Gönen, S., Martínez-Miranda, L.J., Hoag, S.W., 2001. Influence of various drugs on the glass transition temperature of poly(vinylpyrrolidone): a thermodynamic and spectroscopic investigation. Int. J. Pharm. 225, 83-96.
Nagalakshmi, K., Sujatha, S., Alwin, D.,, 2017. DDA loaded PCL nanoparticles enhances the oral bioavailability of DDA in diabetes induced experimental rats. Int. J. Pharm. Pharm. Sci. 9.
Nasrollahzadeh, M., Sajadi, S.M., Sajjadi, M., Issaabadi, Z., 2019. An introduction to nanotechnology. Interface Science and Technology. Elsevier 1–27.
Nathan, D.M., 1993. Long-term complications of diabetes mellitus. N. Engl. J. Med. 328, 1676–1685.
Nauck, M.A., 2014. Update on developments with SGLT2 inhibitors in the management of type 2 diabetes. Drug Des. Devel. Ther. 8, 1335.
Nie, X., Chen, Z., Pang, L., Wang, L., Jiang, H., Chen, Y., Zhang, Z., Fu, C., Ren, B., Zhang, J., 2020. Oral Nano Drug Delivery Systems for the Treatment of Type 2 Diabetes Mellitus: An Available Administration Strategy for Antidiabetic Phytocompounds. Int J Nanomedicine 15.
Niguram, P., Polaka, S.N., Rathod, R., Kalia, K., Kate, A.S., 2020. Update on compatibility assessment of empagliflozin with the selected pharmaceutical excipients employed in solid dosage forms by thermal, spectroscopic and chromatographic techniques. Drug. Dev. Ind. Pharm. 46, 209–218.
Ogueri, K.S., Laurencin, C.T., 2020. Nanofiber Technology for Regenerative Engineering. ACS Nano 14, 9347–9363.
Padmaja, N., Desalegn, T., Sharathbabu, M., Veerabhadram, G., 2018. New validated RP-HPLC method for the estimation of empagliflozin in human plasma. Int. J. Pharm. Sci. 9, 4885–4889.
Pahel, G., Yang, B., Chen, L., Carrick, K., Clifton, L., Mcnulty, J., Winegar, D., Strum, J., Brown, K., Stimpson, S., 2004. Serum Adiponectin as a Biomarker for In Vivo PPARγ Activation and PPARγ Agonist-Induced Efficacy on Insulin Sensitization/Lipid Lowering. Diabetes 53.
Pamuła, E., Błażewicz, M., Paluszkiewicz, C., Dobrzyński, P., 2001. FTIR study of degradation products of aliphatic polyesters–carbon fibres composites. J. Mol. Struct. 596, 69–75.
Pandey, S.P., Shukla, T., Dhote, V.K., Mishra, D.K., Maheshwari, R., Tekade, R.K., 2019. Use of polymers in controlled release of active agents, Basic Fundamentals of Drug Delivery. Elsevier, pp. 113-172.
Panić, J., Vraneš, M., Mirtič, J., Korošec, R.C., Zupančič, Š., Gadžurić, S., Kristl, J., Bešter-Rogač, M., 2022. Preparation and characterization of innovative electrospun nanofibers loaded with pharmaceutically applicable ionic liquids. Int. J. Pharm. 615, 121510.
Papadopoulos, A.N., Taghiyari, H.R., 2019. Innovative wood surface treatments based on nanotechnology. Coatings 9, 866.
Park, H.J., Han, H., Oh, E.-Y., Kim, S.R., Park, K.H., Lee, J.-H., Park, J.-W., 2019. Empagliflozin and dulaglutide are effective against obesity-induced airway hyperresponsiveness and fibrosis in a murine model. Sci. Rep. 9, 1–8.
Park, K., 2007. Nanotechnology: What it can do for drug delivery. J. Control. Release 120, 1.
Partheniadis, I., Athanasiou, K., Laidmäe, I., Heinämäki, J., Nikolakakis, I., 2022. Physicomechanical characterization and tablet compression of theophylline nanofibrous mats prepared by conventional and ultrasound enhanced electrospinning. Int. J. Pharm. 616, 121558.
Pedersen, M., Bruunsgaard, H., Weis, N., Hendel, H.W., Andreassen, B.U., Eldrup, E., Dela, F., Pedersen, B.K., 2003. Circulating levels of TNF-alpha and IL-6-relation to truncal fat mass and muscle mass in healthy elderly individuals and in patients with type-2 diabetes. Mech. Ageing Dev. 124, 495–502.
Ramakrishna, S., 2005. An introduction to electrospinning and nanofibers. World Scientific.
Rashahmadi, S., Hasanzadeh, R., Mosalman, S., 2017. Improving the mechanical properties of poly methyl methacrylate nanocomposites for dentistry applications reinforced with different nanoparticles. Polym. Plast. Technol. Eng. 56, 1730–1740.
Scheen, A.J., 2015. Pharmacodynamics, efficacy and safety of sodium–glucose co-transporter type 2 (SGLT2) inhibitors for the treatment of type 2 diabetes mellitus. Drugs 75, 33–59.
Shahriar, S., Mondal, J., Hasan, M.N., Revuri, V., Lee, D.Y., Lee, Y.-K., 2019. Electrospinning nanofibers for therapeutics delivery. Nanomaterials 9, 532.
Shao, S., Li, L., Yang, G., Li, J., Luo, C., Gong, T., Zhou, S., 2011. Controlled green tea polyphenols release from electrospun PCL/MWCNTs composite nanofibers. Int. J. Pharm. 421, 310–320.
Shewamene, Z., Abdelwuhab, M., Birhanu, Z., 2015. Methanolic leaf exctract of Otostegia integrifolia Benth reduces blood glucose levels in diabetic, glucose loaded and normal rodents. BMC Complement. Altern. Med. 15, 1–7.
Shimko, D.A., Nauman, E.A., 2007. Development and characterization of a porous poly (methyl methacrylate) scaffold with controllable modulus and permeability. J. Biomed. Mater. Res. Part B: Appl. Biomater.: Off. J. Soc. Biomater. Jpn. Soc. Biomater. Austral. Soc. Biomater. Kor. Soc. Biomater. 80, 360–369.
Sperling, L.E., Reis, K.P., Pranke, P., Wendorff, J.H., 2016. Advantages and challenges offered by biofunctional core–shell fiber systems for tissue engineering and drug delivery. Drug Discov. Today 21, 1243–1256.
Steven, S., Oelze, M., Hanf, A., Kröller-Schön, S., Kashani, F., Roohani, S., Welschof, P., Kopp, M., Gödtel-Armbrust, U., Xia, N., 2017. The SGLT2 inhibitor empagliflozin improves the primary diabetic complications in ZDF rats. Redox Biol. 13, 370–385.
Stewart, J.E., Wager, K.A., Friedlander, A.H., Zadeh, H.H., 2001. The effect of periodontal treatment on glycemic control in patients with type 2 diabetes mellitus. J. Clin. Periodontol. 28, 306–310.
Tang, Z., Callaghan, J., Hunt, J., 2005. The physical properties and response of osteoblasts to solution cast films of PLGA doped polycaprolactone. Biomaterials 26, 6618–6624.
Teo, W.E., Ramakrishna, S., 2006. A review on electrospinning design and nanofibre assemblies. Nanotechnology 17, R89.
Tikkanen, I., Narko, K., Zeller, C., Green, A., Salsali, A., Broedl, U.C., Woerle, H.J., 2015. Empagliflozin reduces blood pressure in patients with type 2 diabetes and hypertension. Diabetes Care 38, 420–428.
Tornehave, D., Kristensen, P., Rømer, J., Knudsen, L.B., Heller, R.S., 2008. Expression of the GLP-1 receptor in mouse, rat, and human pancreas. J. Histochem. Cytochem. 56, 841–851.
Uranga, R.M., Millán, C., Barahona, M.J., Recabal, A., Salgado, M., Martinez, F., Ordenes, P., Elizondo-Vega, R., Sepúlveda, F., Uribe, E., 2017. Adenovirus-mediated suppression of hypothalamic glucokinase affects feeding behavior. Sci. Rep. 7, 1–13.
Verma, P., Thakur, A., Deshmukh, K., Jha, A., Verma, S., 2010. Routes of drug administration. Int. J. Pharm. Sci. Res. 1, 54–59.
Wachirahuttapong, S., Thongpin, C., Sombatsompop, N., 2016. Effect of PCL and compatibility contents on the morphology, crystallization and mechanical properties of PLA/PCL blends. Energy Procedia 89, 198–206.
Wang, M., Ge, R., Zhao, P., Williams, G.R., Yu, D.-G., Bligh, S.W.A., 2023. Exploring wettability difference-driven wetting by utilizing electrospun chimeric Janus microfiber comprising cellulose acetate and polyvinylpyrrolidone. Mater. Des. 226, 111652.
Wang, M., Hou, J., Yu, D.-G., Li, S., Zhu, J., Chen, Z., 2020. Electrospun tri-layer nanodepots for sustained release of acyclovir. Journal of Alloys and Compounds 846, 156471.
Wong, S.-C., Baji, A., Leng, S., 2008. Effect of fiber diameter on tensile properties of electrospun poly (ε-caprolactone). Polymer 49, 4713–4722.
Xie, C., Yan, J., Cao, S., Liu, R., Sun, B., Xie, Y., Qu, K., Zhang, W., Weng, Z., Wang, Z., 2022. Bi-layered disulfiram-loaded fiber membranes with antibacterial properties for wound dressing. Appl. Biochem. Biotechnol. 194, 1359–1372.
Xu, G., Kaneto, H., Lopez-Avalos, M.D., Weir, G.C., Bonner-Weir, S., 2006. GLP-1/exendin-4 facilitates β-cell neogenesis in rat and human pancreatic ducts. Diabetes Res. Clin. Pract. 73, 107–110.
Xu, Z., Li, J., Zhou, H., Jiang, X., Yang, C., Wang, F., Pan, Y., Li, N., Li, X., Shi, L., 2016. Morphological and swelling behavior of cellulose nanofiber (CNF)/poly (vinyl alcohol)(PVA) hydrogels: poly (ethylene glycol)(PEG) as porogen. RSC Adv. 6, 43626–43633.
Yu, D.-G., Li, Q., Song, W., Xu, L., Zhang, K., Zhou, T., 2023. Advanced technique-based combination of innovation education and safety education in higher education. J. Chem. Educ.
Zghebi, S.S., Steinke, D.T., Carr, M.J., Rutter, M.K., Emsley, R.A., Ashcroft, D.M., 2017. Examining trends in type 2 diabetes incidence, prevalence and mortality in the UK between 2004 and 2014. Diabetes Obes. Metab. 19, 1537–1545.

Zhao, K., Lu, Z.-H., Zhao, P., Kang, S.-X., Yang, Y.-Y., Yu, D.-G., 2021. Modified tri–axial electrospun functional core–shell nanofibrous membranes for natural photodegradation of antibiotics. Chem. Eng. J. 425, 131455.

Zhou, Y., Wang, M., Yan, C., Liu, H., Yu, D.-G., 2022. Advances in the Application of Electrospun Drug-Loaded Nanofibers in the Treatment of Oral Ulcers, Biomolecules.

Zong, X., Ran, S., Kim, K.-S., Fang, D., Hsiao, B.S., Chu, B., 2003. Structure and morphology changes during in vitro degradation of electrospun poly (glycolide-co-lactide) nanofiber membrane. Biomacromolecules 4, 416–423.